The contribution of massive haloes to the matter power spectrum in the presence of AGN feedback
Loon, M.L. van; Daalen, M.P. van

Citation
Loon, M. L. van, & Daalen, M. P. van. (2024). The contribution of massive haloes to the matter power spectrum in the presence of AGN feedback. *Monthly Notices Of The Royal Astronomical Society*, *528*(3), 4623-4642. doi:10.1093/mnras/stae285

Version: Publisher's Version
License: Creative Commons CC BY 4.0 license
Downloaded from: https://hdl.handle.net/1887/4179326

Note: To cite this publication please use the final published version (if applicable).

Monthly Notices of the ROYAL ASTRONOMICAL SOCIETY

MNRAS **528,** 4623–4642 (2024) https://doi.org/10.1093/mnras/stae285
Advance Access publication 2024 January 27

The contribution of massive haloes to the matter power spectrum in the presence of AGN feedback

M. L. van Loon★ and Marcel P. van Daalen
Leiden Observatory, Leiden University, P. O. Box 9513, NL-2300 RA Leiden, the Netherlands

Accepted 2024 January 25. Received 2024 January 10; in original form 2023 September 14

ABSTRACT

The clustering of matter, as measured by the matter power spectrum, informs us about cosmology, dark matter, and baryonic effects on the distribution of matter in the universe. Using cosmological hydrodynamical simulations from the cosmo-OWLS and BAHAMAS simulation projects, we investigate the contribution of power in haloes with various masses, to the full power spectrum, as well as the power ratio between baryonic and dark matter only (DMO) simulations for a matched (between simulations) and an unmatched set of haloes. We find that the presence of AGN feedback suppresses the power on all scales for haloes of all masses examined ($10^{11.25} \leq M_{500,\,\rm crit} \leq 10^{14.75}\,\mathrm{M}_{\odot}/h$), by ejecting matter from within $r_{500,\rm c}$ to $r_{200,\rm m}$ and potentially beyond in massive haloes ($M_{500,\,\rm crit} \gtrsim 10^{13}\,\mathrm{M}_{\odot}/h$), and likely impeding the growth of lower-mass haloes as a consequence. A lower AGN feedback temperature changes the behaviour of high-mass haloes ($M_{500,\,\rm crit} \geq 10^{13.25}\,\mathrm{M}_{\odot}/h$), damping the effects of AGN feedback at small scales, $k \gtrsim 4\,h\,\mathrm{Mpc}^{-1}$. For $k \lesssim 3\,h\,\mathrm{Mpc}^{-1}$, group-sized haloes ($10^{14\pm0.25}\,\mathrm{M}_{\odot}/h$) dominate the power spectrum, while on smaller scales the combined contributions of lower-mass haloes to the full power spectrum rise above that of the group-sized haloes. Finally, we present a model for the power suppression due to feedback, which combines observed mean halo baryon fractions with halo mass fractions and halo-matter cross-spectra extracted from DMO simulations to predict the power suppression to per cent level accuracy down to $k \approx 10\,h\,\mathrm{Mpc}^{-1}$ without any free parameters.

Key words: cosmology: theory – large-scale structure of Universe – galaxies: formation – galaxies: haloes – gravitational lensing: weak.

1 INTRODUCTION

Understanding the way matter clusters is an integral piece in furthering our knowledge about the universe and its inner workings. The clustering of matter governs halo collapse and galaxy formation, along with mergers and other processes. All these processes are heavily dependent on the cosmological parameters, the fundamental parameters describing our Universe. These parameters dictate, among other things, the matter density of the universe, its expansion, and, by extension, how much of the matter is formed into haloes and galaxies, along with their formation time-scales.

Although the ΛCDM model is the most widely established cosmological model, incorporating cold dark matter and dark energy, its parameters are not set. Observational data from the two largest cosmological probes, the Wilkinson Microwave Anisotropy Probe (WMAP) (see Komatsu et al. 2011; Hinshaw et al. 2013, for the 7- and 9-yr results, respectively) and *Planck* (see Ade et al. 2014; *Planck* Collaboration et al. 2016, for the 2013 and 2015 releases, respectively), provide measurements of the cosmic microwave background (CMB) from which the cosmology of our Universe can be derived, but there is growing evidence that there is tension between these early-universe probes and late-universe measurements (see Abdalla et al. 2022, for a recent review). The latter type of measurements typically study some aspect of the clustering of matter, for example through weak gravitational lensing (e.g. Heymans et al. 2021; Abbott et al. 2022), and compare this to theoretical models to derive cosmology. One particular measure of clustering is the matter power spectrum, generally given as $P(k)$ (or $\Delta^2(k)$): the amplitude squared of matter overdensities as a function of Fourier scale, k, which is given by $2\pi/\lambda$, where λ refers to the physical scale.

On the largest scales, linear perturbation theory is sufficient to model the power spectrum, originally proposed by Press & Schechter (1974) and extended by Bond et al. (1991). However, on smaller, non-linear scales, governing halo collapse and galaxy formation, linear theory underestimates the power and additional physics needs to be taken into account. A widely accepted model incorporating non-linear scales is the analytical halo model (e.g. Peacock & Smith 2000; Seljak 2000; Cooray & Sheth 2002), which has been added to by many others (e.g. Duffy et al. 2008; Tinker et al. 2008; Semboloni, Hoekstra & Schaye 2013; Mead et al. 2015; Debackere, Schaye & Hoekstra 2020; Mead et al. 2021). As future weak lensing surveys, enabling high-precision (< 1 per cent) measurements of (matter) power spectra, draw near, the importance of theoretical understanding and predictions on these non-linear scales increases (e.g. Huterer & Takada 2005; Laureijs 2009; Hearin, Zentner & Ma 2012).

Currently, the precise effects of baryons, for example through galaxy formation and evolution, on the matter power spectrum (hereafter referred to as: power spectrum) are still largely undetermined

★ E-mail: mvanloon98@gmail.com

© 2024 The Author(s)
.Published by Oxford University Press on behalf of Royal Astronomical Society. This is an Open Access article distributed under the terms of the Creative Commons Attribution License (https://creativecommons.org/licenses/by/4.0/), which permits unrestricted reuse, distribution, and reproduction in any medium, provided the original work is properly cited

Downloaded from https://academic.oup.com/mnras/article/528/3/4623/7590824 by Jacob Heeren user on 07 February 2025

(see Chisari et al. 2019, for a review). Countless complex and coupled processes underlie the formation and evolution of galaxies that often play out on small, not directly observable, scales. Hydrodynamical, cosmological simulations, which can produce a statistically interesting sample of realistic galaxies, offer insights and help to determine which theoretical models best describe observations or which observations are predicted based on theory. The trade-off between resolution and sample size remains a challenge, although increased computational efficiency and so-called 'subgrid models', which allow unresolved physical processes to be taken into account, have come a long way in the last few decades (for a review, see Vogelsberger et al. 2020).

The widely accepted idea that the clustering of all matter is fully determined by that of dark matter was refuted when van Daalen et al. (2011) found that the presence of AGN feedback has a profound impact on the power spectrum, using simulations from the OWLS project (Schaye et al. 2010). Not only is there an effect on the clustering of baryons by the material that is ejected out to large radii, the dark matter reacts to these changes by expanding, a phenomenon dubbed 'the back reaction' (e.g. Duffy et al. 2010; van Daalen et al. 2011; Velliscig et al. 2014a). This suppression of the power spectrum has been confirmed and/or modelled by others since then (e.g. Vogelsberger et al. 2014; Mead et al. 2015; Hellwing et al. 2016; Mummery et al. 2017; Chisari et al. 2018; Schneider et al. 2019; Aricò et al. 2021; Pandey et al. 2023; Salcido et al. 2023). However, the mechanisms causing AGN feedback and the consequences on the surrounding material are as of yet inadequately understood in the context of the power spectrum to predict the power spectrum to near 1 per cent accuracy over a sufficient range of scales based solely on cosmology (e.g. van Daalen, McCarthy & Schaye 2020).

In order to make valid predictions of the power spectrum, we need to understand which parts of the matter distribution contribute significantly to the full power spectrum on any given scale. One way to separate the power spectrum into components, is to distinguish between the contributions to the full power spectrum of autopower produced by haloes only, autopower generated by matter not in haloes and cross-power between halo and non-halo matter. The contribution of these components is influenced by the definition of halo boundary used in a scale-dependent way, as found by van Daalen & Schaye (2015) for the halo autopower spectrum in dark matter only (DMO) simulations.

Keeping a consistent definition for halo boundaries, e.g. a radius marking a spherical overdensity (SO) region, separate power spectra for haloes of certain masses can be considered, to explore their individual or combined effects to the full power spectrum. Therefore, van Daalen & Schaye (2015) considered the contribution of power in haloes to the full power spectrum in DMO simulations for a varying minimum halo mass. They found that group-sized haloes (with $M_{200,\,\mathrm{mean}} \gtrsim 10^{13.75}\,\mathrm{M_\odot}/h$) are the main contributors to matter clustering for $2 \lesssim k \lesssim 10\,h\,\mathrm{Mpc}^{-1}$, even though they contain only $\sim$ 13 per cent of the total mass. The deviation between the mass fraction and the contribution to the total power stems from the interplay between the rarity of massive haloes, lowering their contribution to the total power, and the deeper potential wells of massive haloes, which result in increased clustering of the matter, along with their already more clustered environments (i.e. their bias), raising their contribution to the total power (see also e.g. Debackere et al. (2020). Even so, van Daalen & Schaye (2015) found that a significant (> 1 per cent) amount of power is still provided by unresolved haloes ($M_{200,\,\mathrm{mean}} \lesssim 10^{9.5}\,\mathrm{M_\odot}/h$) and, potentially, smooth dark matter.

The relevance of the large contribution of group-sized haloes to matter clustering was further confirmed when van Daalen et al. (2020) examined a library of 92 power spectra for cosmological simulations using different galaxy formation models and parameters. They found that the mean baryon fraction of these ($M \sim 10^{14}\,\mathrm{M_\odot}/h$) haloes can be used to predict the power suppression due to galaxy formation to typically within 1 per cent for $k < 1\,h\,\mathrm{Mpc}^{-1}$.

Considering the importance of group-sized haloes to clustering measurements and the studying of other physical processes (e.g. McCarthy et al. 2010; Oppenheimer et al. 2021), here we delve deeper into the role of these objects in shaping the power spectrum. To this end we utilize the cosmo-OWLS (Le Brun et al. 2014; McCarthy et al. 2014) and BAHAMAS (BAryons and haloes of MAssive Systems, McCarthy et al. 2017) simulations, which were made to study haloes of these masses, and try to quantify the impact of AGN feedback on the contribution of (group-sized) haloes to the power spectrum. Furthermore, we explore the influence of AGN feedback on the suppression of power on smaller scales for different components of the power spectrum, creating a model, based on the key element of mass removal from clustered regions, that can predict this suppression to per cent level accuracy down to $k \approx 10\,h\,\mathrm{Mpc}^{-1}$ in a way that is independent of the galaxy formation recipes used. By furthering our understanding of the contributions haloes of different masses have, and the effects of baryonic feedback processes, we hope this work can provide a stepping stone for future research to increase the precision of theoretical power spectrum predictions on non-linear scales.

This paper is structured as follows. In Section 2, we describe the simulations in more detail, and provide a formal definition of the power spectrum and other methods used to obtain the results. Then, Section 3 describes the results, where the contributions of halo autopower for an unmatched set of $r_{200,\mathrm{m}}$ haloes is considered in subsection 3.1. The halo autopower for a matched set of haloes is similarly considered in subsection 3.2. Using this same matched catalogue, we also explore the clustering contributions of $r_{500,\mathrm{c}}$ SO regions instead (subsection 3.3), consider the results when using a fixed SO radius between simulations (subsection 3.4), and investigate the effects of varying the AGN feedback temperature (subsection 3.5). The effects of cosmology on the results is briefly discussed in Appendix B. Other contributions to the power spectrum, that is, cross terms, are considered in subsection 3.6, based on which we derive a model for power suppression in Section 4. Finally, Section 5 provides a summary of our results and a brief discussion of the model's potential.

2 METHODS

2.1 Measurements and data

2.1.1 Simulations

The results in Section 3 are based on a set of simulations from the cosmo-OWLS (Le Brun et al. 2014) and BAHAMAS (McCarthy et al. 2017) simulation projects, which were designed to study group- and cluster-sized haloes. Both projects were run on a modified version of GADGET-3, with smoothed particle hydrodynamics (SPH), as described by Springel (2005). The relevant simulation parameters are listed in Table 1 along with the abbreviations of the simulation names, which will be used in the rest of the paper to refer to the simulations.

All simulations used in this study have a volume of $(400\,h^{-1}\,\mathrm{Mpc})^3$ and 1024^3 particles ($\times$ 2 for simulations including baryons, or 2-fluid DMO simulations). These are therefore generally indicated with the suffix L400N1024, but for brevity we will omit this suffix

Downloaded from https://academic.oup.com/mnras/article/528/3/4623/7590824 by Jacob Heeren user on 07 February 2025

Table 1. Relevant simulation parameters for simulations from BAHAMAS (McCarthy et al. 2017) and cosmo-OWLS (Le Brun et al. 2014) that are used in this research. Simulation names (and their abbreviations) include the cosmologies used, along with particle types present (DMO only contains dark matter, REF, and AGN are baryonic). All simulations have volumes ($400\,h^{-1}$ Mpc)^3. The AGN simulations include thermal AGN feedback, with heating temperature $\Delta T_{\rm heat}$, REF only has SN feedback.

Name	Abbreviation	$m_{\rm dm}$ [h^{-1} M$_\odot$]	$m_{\rm bar,\,initial}$ [h^{-1} M$_\odot$]	$\Delta T_{\rm heat}$
C-OWLS_DMONLY_WMAP7	C_DMO_W7	4.50×10^9	–	–
C-OWLS_REF_WMAP7	C_REF_W7	3.75×10^9	7.54×10^8	–
C-OWLS_AGN_WMAP7	C_AGN_W7	3.75×10^9	7.54×10^8	$10^{8.0}$ K
BAHAMAS_DMONLY_2fluid_nu0_WMAP9	B_DMO_W9	3.85×10^9	7.66×10^8	–
BAHAMAS_nu0_WMAP9	B_AGN_W9	3.85×10^9	7.66×10^8	$10^{7.8}$ K
BAHAMAS_Theat7.6_nu0_WMAP9	B_AGNlow_W9	3.85×10^9	7.66×10^8	$10^{7.6}$ K
BAHAMAS_Theat8.0_nu0_WMAP9	B_AGNhigh_W9	3.85×10^9	7.66×10^8	$10^{8.0}$ K
BAHAMAS_DMONLY_2fluid_nu0_Planck2013	B_DMO_PL	4.44×10^9	8.11×10^8	–
BAHAMAS_nu0_Planck2013	B_AGN_PL	4.44×10^9	8.11×10^8	$10^{7.8}$ K

Table 2. Cosmological parameters from the seven-year WMAP release (Komatsu et al. 2011), the nine-year WMAP release (Hinshaw et al. 2013), and the 2013 *Planck* release (Ade et al. 2014) used in the simulations from Table 1.

	$\Omega_{\rm m}$	$\Omega_{\rm b}$	Ω_Λ	σ_8	n_s	h
WMAP7	0.272	0.0455	0.728	0.81	0.967	0.704
WMAP9	0.2793	0.0463	0.7207	0.821	0.972	0.700
Planck	0.3175	0.0490	0.6825	0.834	0.9624	0.6711

everywhere, except in Appendix A, which studies box-size effects on the results at a constant resolution. The DMO simulations, as the name indicates, include only dark matter particles. In the REF simulation (cosmo-OWLS), gas and star particles and their relevant physics (e.g. star formation, metal enrichment, supernova feedback) have been added, and the AGN simulations add supermassive black hole particles along with their accretion and feedback to the mix, which are seeded into haloes with >100 dark matter particles. The particle masses are listed in Table 1. The doubling of the number of particles, along with the mass difference between them in a DMO and a baryonic simulation, causes a variation in resolution effects between these simulations on small scales, which also affects the matter clustering. Therefore, in the BAHAMAS project, the 2-fluid DMO simulations split every dark matter particle into two dark matter particles, with the dark matter–baryon mass ratio, and use a separate transfer function for each, to account for this effect and make a comparison on smaller scales between DMO and baryonic simulations more easily interpretable.

For the cosmo-OWLS simulations, the seven-year WMAP cosmological parameters are used (WMAP7, Komatsu et al. 2011), as listed in Table 2. The BAHAMAS simulations use the newer, nine-year WMAP results (WMAP9, Hinshaw et al. 2013), also listed in Table 2. To investigate whether our results show a dependence on cosmology, these simulations are compared to the simulations run with the 2013 *Planck* cosmological parameters (Ade et al. 2014, named '*Planck*' in Table 2) in fig. B1 of Appendix B.

Starting from initial conditions generated by V. Springel's software package N-GENIC [1], which was updated to include second-order Lagrangian Perturbation Theory by S. Bird for BAHAMAS, and using a transfer function as prescribed by Eisenstein & Hu (1999) (cosmo-OWLS) or the Boltzmann code CAMB [2] (Lewis, Challinor & Lasenby 2000) (BAHAMAS), the particles in the simulations are evolved to $z = 0$ by solving the relevant gravitational and hydrodynamical equations, and 'sub-grid' models, describing unresolved, but relevant, physics. The sub-grid models for both cosmo-OWLS and BAHAMAS are identical and include radiative heating and cooling rates, which are interpolated from pre-computed results from CLOUDY results (see Wiersma, Schaye & Smith 2009, for details); an effective equation of state to govern cold gas in the interstellar medium, including a density threshold for possible star formation, which is in turn implemented by a stochastic model. Furthermore, there are models to describe stellar evolution, chemical enrichment and stellar feedback, along with procedures for the accretion and mergers of supermassive black holes and the resulting AGN feedback. All the sub-grid model parameters have been calibrated using the local Galaxy Stellar Mass Function (GSMF) (for an extended description of the models and the calibration see Schaye et al. 2010; Le Brun et al. 2014; McCarthy et al. 2017).

All sub-grid model parameters are identical between cosmo-OWLS and BAHAMAS with the exception of baryonic feedback, that is, supernova (SN) and AGN feedback, where the parameters in the latter simulation set have been tweaked to better match hot gas fraction observations of groups and clusters, in addition to the GSMF. In their AGN simulations, cosmo-OWLS and BAHAMAS both use thermal AGN feedback, which entails that the feedback is'accumulated' in the black hole until 1 (cosmo-OWLS) or 20 (BAHAMAS) surrounding particle(s) can be heated by $\Delta T_{\rm heat}$. This heating temperature is a model parameter, shown in Table 1, that is varied between simulations, as its 'true' value is unknown. Since the $\Delta T_{\rm heat}$ parameter only weakly influences the produced GSMF, it has been calibrated using the hot gas fractions of groups and clusters after the other feedback model parameters had been set. For the BAHAMAS simulations, this resulted in a change of this parameter from $\Delta T_{\rm heat} = 10^{8.0}\,K$, as in the original cosmo-OWLS, to $\Delta T_{\rm heat} = 10^{7.8}\,K$, to better match hot gas fraction observations (see McCarthy et al. 2017, for details). Runs with the original ($10^{8.0}$) and a slightly lower ($10^{7.6}$) $\Delta T_{\rm heat}$ have been included in BAHAMAS to study the effect of the parameter, which resembles feedback strength. The cosmo-OWLS 'reference' (REF) simulations include SN feedback but not AGN feedback, causing the well-known 'overcooling' problem (see McCarthy et al. 2010, 2011).

2.1.2 Power spectra

Recall from Section 1 that the power spectrum can be seen as the amplitude squared of the Fourier transform of the matter overdensity field. Most of our results will be shown in terms of the power

[1] http://www.mpa-garching.mpg.de/gadget/
[2] http://camb.info/

Downloaded from https://academic.oup.com/mnras/article/528/3/4623/7590824 by Jacob Heeren user on 07 February 2025

spectrum, defined as

$$P(k) = V \left\langle |\hat{\delta}_{\mathbf{k}}|^2 \right\rangle_{\mathrm{k}}, \quad (1)$$

where k is the Fourier scale, P is the power, V the volume of the simulation (which is $(400\,h^{-1}\mathrm{Mpc})^3$ everywhere) and $\hat{\delta}_{\mathbf{k}}$ is the Fourier transform of the density contrast. In Fig. 2, an exception is made and $P(k)k^{1.5}$ is shown to take out the main k-dependence and make the comparison between lines easier. The shot noise, generated by the 'clustering' of particles with themselves, is subtracted from the power to account for the discreteness of the density field.

All autopower spectra are calculated using a modified version of POWMES (as described in van Daalen & Schaye 2015 Bsemi see Colombi et al. 2009 for the original version), which takes as input a particle selection, along with a list of parameters and a path to the simulation data, and outputs the power at each scale.

The cross-power spectra, used in subsection 3.6 and Section 4, are calculated using NBODYKIT (see Hand et al. 2018, for a detailed description).

2.1.3 Selections

For the results in Section 3, the SUBFIND output of the simulations is first used to divide the haloes based on mass, whereafter the bound and spherical overdensity particles are selected based on their radial distance to the centre of the halo, using PYTHON.

The haloes are defined using cut-off radii where either $r_{200,\mathrm{m}}$ or $r_{500,\mathrm{c}}$ is chosen, corresponding to the radii wherein the average density is equal to 200 times the mean density ($200 \times \Omega_{\mathrm{m}}\rho_{\mathrm{crit}}$) or 500 times the critical density ($500 \times \rho_{\mathrm{crit}}$), respectively. However, in order to enable comparison between figures, the halo mass we select on is always chosen as the mass within $r_{500,\mathrm{c}}$ ($M_{500,\,\mathrm{crit}} = 500 \times \frac{4\pi}{3}\rho_{\mathrm{crit}} r_{500,\mathrm{c}}{}^3$), regardless of the SO region used in particle selection. Furthermore, a cutoff of 100 particles is enforced to counter resolution effects. This mostly affects the lowest mass bin of figures where haloes are matched between simulations (see subsection 2.2) because not all haloes containing >100 particles have a >100 particle match.

The halo mass bins range from $M_{500,\,\mathrm{crit}} = 10^{11.25}\,\mathrm{M}_{\odot}/h$ to $M_{500,\,\mathrm{crit}} = 10^{14.75}\,\mathrm{M}_{\odot}/h$ with a width of 0.5 dex, to reduce mass evolution effects within the mass bin, while ensuring a large enough sample size. For the figures where haloes are matched between simulations (see Section 2.2), the halo mass selection is based on the DMO simulation masses, contrary to the unmatched figures where the masses correspond to the simulation shown.

2.2 Matching

For some figures in Section 3 (e.g. Fig. 4), the haloes are matched between simulations, which is made possible by the initial conditions of simulations in the same set being identical. For cosmo-OWLS, two sets of matches were made: haloes in C_DMO_W7 were matched with their equivalents in C_AGN_W7, and separately with their haloes in C_REF_W7, for each box size (L100, L200, L400), for halo masses $10^{11.25}\,\mathrm{M}_{\odot}/h$ and up. For BAHAMAS, the following sets of matches were made: B_DMO_W9–B_AGN_W9, B_DMO_W9–B_AGNlow_W9, B_DMO_W9–B_AGNhigh_W9, and B_DMO_PL–B_AGN_PL, for halo masses $\geq 10^{11.25}\,\mathrm{M}_{\odot}/h$. A match between B_DMO_W9 and B_DMO_PL for halo masses $\geq 10^{11.25}\,\mathrm{M}_{\odot}/h$ was also made, to allow for a comparison between cosmologies (see Appendix B).

During the matching, the particle IDs of the 100 most-bound dark matter particles of each halo within the mass range in the DMO simulation, are compared to all the dark matter IDs of the haloes in the same or a neighbouring grid section in the other simulation. The halo where most of these particles are found is placed in a list, where a minimum of 50 particles is required to be considered a match. The particles of the 100 most-bound dark matter particles of these haloes are then found in the DMO simulation in the same way. Furthermore, a halo position check ensures that the matched haloes are < 1 Mpc apart. In the BAHAMAS matching, the computing time is sped up by also imposing a mass limit of a factor 5 within the mass of the halo for haloes in neighbouring grid sections. If a halo pair passes these tests it is considered a match and the index pair is saved.

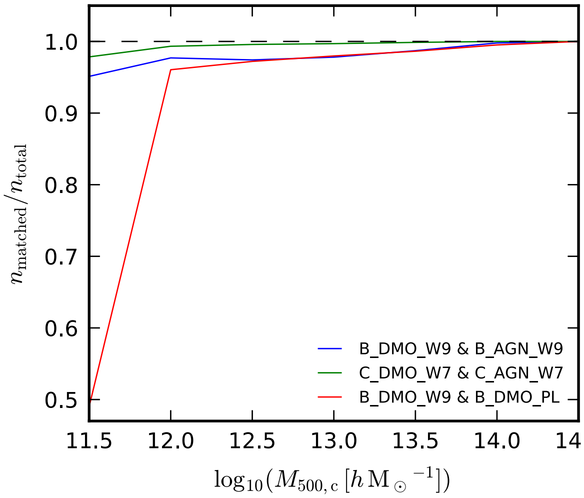

Figure 1. The fraction of matched haloes out of the total number per halo mass bin (width 0.5 dex) for the match between B_DMO_W9 and B_AGN_W9 (blue), between C_DMO_W7 and C_AGN_W7 (green), and between B_DMO_PL and B_DMO_W9 (red). With the exception of the lowest mass bin in the cosmology match ($M_{500,\,\mathrm{crit}} = 10^{11.5\pm0.25}\,\mathrm{M}_{\odot}/h$), all match fractions are >0.95.

The fraction of matched haloes as a function of halo mass is given in Fig. 1 for the match between B_DMO_W9 and B_AGN_W9 (blue line, representative for all BAHAMAS DMO–baryon pairs), the match between C_DMO_W7 and C_AGN_W7 (green), and the match between B_DMO_W9 and B_DMO_PL (red) used in subsection 3.2. For $M_{500,\,\mathrm{crit}} \geq 10^{11.75}\,\mathrm{M}_{\odot}/h$, the matched fraction is >0.95 for all pairs. For the lowest mass bin ($M_{500,\,\mathrm{crit}} = 10^{11.5\pm0.25}\,\mathrm{M}_{\odot}/h$) the matched fraction between different cosmologies is ∼0.5, calling for caution in the interpretation.

During the selection of particles for POWMES or NBODYKIT (as described in subsection 2.1.3), the haloes are selected based on their DMO-simulation masses, and only matched haloes are considered. For the results in subsection 3.4, the SO region radii from the corresponding haloes in the DMO simulation are taken as a selection criterion for the AGN simulation haloes.

3 RESULTS

When considering the effects of galaxy formation on the theoretical power spectrum, it is common to consider the ratio of a power spectrum from a hydrodynamical simulation to that of a DMO simulation, so that small (but relevant) deviations from unity become more apparent (see e.g. fig. 2 of van Daalen et al. 2020). In general, the shape of this ratio is a dip downwards from unity for $k \gtrsim 0.1\,h\,\mathrm{Mpc}^{-1}$, meaning the power in realistic simulations is

Downloaded from https://academic.oup.com/mnras/article/528/3/4623/7590824 by Jacob Heeren user on 07 February 2025

power spectrum. Therefore, this section focuses on the contributions of a range of halo masses to the full spectrum and the ratio between baryon and DMO simulations to gain more understanding about the role of feedback processes for different halo masses.

3.1 Autopower contributions for non-matched haloes

In this section, the $M_{500,\,\rm crit}$ halo masses include baryons when present in the simulation. Only the three simulations from cosmo-OWLS are used, C_DMO_W7, C_REF_W7, and C_AGN_W7, all with WMAP7 cosmology and the latter two including baryons. Furthermore, the simulations are not matched, resulting in skewed halo distributions in the mass bins between simulations, as AGN feedback lowers halo masses. Subsection 3.2 describes the results that are obtained when the haloes are matched between simulations.

In Fig. 2 the power spectra of simulations C_AGN_W7 (solid), C_DMO_W7 (transparent), and C_REF_W7 (transparent and dashed) are shown for a range of halo mass bins between $10^{11.25}\,\mathrm{M_\odot}/h$ and $10^{14.75}\,\mathrm{M_\odot}/h$ (with a width of 0.5 dex), at $z = 0$. The power spectra are multiplied by $k^{1.5}$ to take out the main k-dependence and to make a comparison between the lines easier.

In the top panel, all particles within $r_{200,\rm m}$ of haloes with masses greater than that indicated in the legend are taken into account. The more haloes are taken into account, the closer the power spectrum is to the full power spectrum (black line). Note that we do not expect to converge to this limit as more haloes are taken into account, since not all matter resides in (resolved, $r_{200,\rm m}$) haloes. For all mass bins, the power spectra have a similar shape: the power increases with k, reaches a maximum at the scale at which the (larger) haloes are entered and then decreases (keeping in mind that we multiply $P(k)$ with $k^{1.5}$ here). The scale at which the haloes are entered becomes larger with increasing halo mass, effectively moving the peak in the figure towards smaller k.

A comparison of simulations reveals a lower power of C_AGN_W7 on large scales, compared to both C_DMO_W7 and C_REF_W7, due to AGN feedback lowering the halo mass. The haloes that are in a certain C_AGN_W7 mass bin, are in in a higher mass bin in the C_DMO_W7 or C_REF_W7 simulations. As low-mass haloes are more numerous than high-mass haloes, more haloes will be included in the C_DMO_W7 and C_REF_W7 mass bins, increasing the power. On smaller scales, C_REF_W7 power increases more strongly due to over cooling while C_AGN_W7 dips under C_DMO_W7 as the effective feedback heats the gas and pushes baryons to larger scales, the dark matter reacting gravitationally.

In the bottom panel of Fig. 2, only particles within $r_{200,\rm m}$ of haloes within the indicated mass bin (width of 0.5 dex) are taken into account. The shapes are similar to the top panel, although a comparison between masses reveals that the power on large and intermediate scales increases with halo mass for haloes with $M_{500,\,\rm crit} \lesssim 10^{14.25}\,\mathrm{M_\odot}/h$. The power of the largest haloes ($M_{500,\,\rm crit} = 10^{14.5\pm0.25}\,\mathrm{M_\odot}/h$, red lines) is lower or equal to the second-largest mass bin ($M_{500,\,\rm crit} = 10^{14\pm0.25}\,\mathrm{M_\odot}/h$, orange lines), as was found previously by van Daalen & Schaye (2015). Although cosmic variance plays a minor role in this (as we checked using three B_AGN_W9 simulations with varying initial conditions, not shown), it is mostly due to cosmic deficiency. In other words, the $10^{14.5\pm0.25}\,\mathrm{M_\odot}/h$ haloes are so rare that their higher mass and bias no longer wins out, lowering their contribution to the full power spectrum relative to slightly less massive haloes.

For low-mass haloes ($M_{500,\,\rm crit} \lesssim 10^{13}\,\mathrm{M_\odot}/h$), the peaks of the autopower spectra from the baryonic simulations lie above those from C_DMO_W7, whereas those for higher mass haloes lie below. The

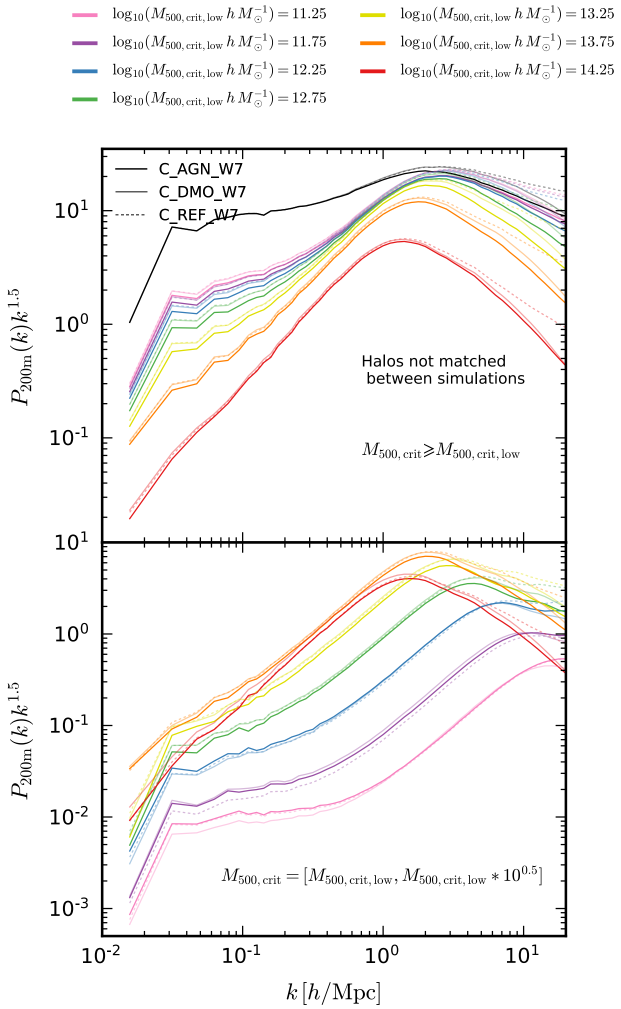

Figure 2. The power spectra of C_AGN_W7 (solid), C_DMO_W7 (transparent), and C_REF_W7 (transparent and dashed) for various halo mass selections, at $z = 0$. The legend shows which $M_{500,\,\rm crit}$ selection is made: $M_{500,\,\rm crit} \geq 10^{x-0.25}\,\mathrm{M_\odot}/h$ (top panel) or $10^{x-0.25}\,\mathrm{M_\odot}/h \leq M_{500,\,\rm crit} \leq 10^{x+0.25}\,\mathrm{M_\odot}/h$ (bottom panel), with x ranging from 11.5 to 15 (see top legend for colour scheme). Only particles within the SUBFIND radius corresponding to a spherical overdensity of $200\bar{\rho}$ ($r = r_{200,\rm m}$) are taken into account. The contribution of haloes with $M_{500,\,\rm crit} = 10^{14\pm0.25}\,\mathrm{M_\odot}/h$ to the full spectrum exceeds the contributions of haloes with other masses at $k < 3\,h\,\mathrm{Mpc}^{-1}$. A comparison between simulations shows that AGN feedback lowers the fraction of mass residing in haloes of all masses, the SO radius, as well as the contribution to the full power spectrum on small scales ($k > 8\,h\,\mathrm{Mpc}^{-1}$) of haloes with $M_{500,\,\rm crit} \gtrsim 10^{11.75}\,\mathrm{M_\odot}/h$.

suppressed on large and intermediate, non-linear scales, relative to a DMO universe, due to matter being removed from clustered regions by feedback processes. This dip flattens out to a suppression of $\sim 10-20$ per cent depending on the model used (with more effective feedback causing a stronger suppression), followed by a sharp upturn for $k \gtrsim 10\,h\,\mathrm{Mpc}^{-1}$ into ratios far above unity on small scales. This upturn is caused by the cooling of the baryons into a central galaxy on even smaller scales, which increases the concentration of the inner dark matter halo.

To more precisely understand the physical processes behind the shape of the power spectrum and its suppression due to feedback, we need to dive deeper into the different contributions that make up the

Downloaded from https://academic.oup.com/mnras/article/528/3/4623/7590824 by Jacob Heeren user on 07 February 2025

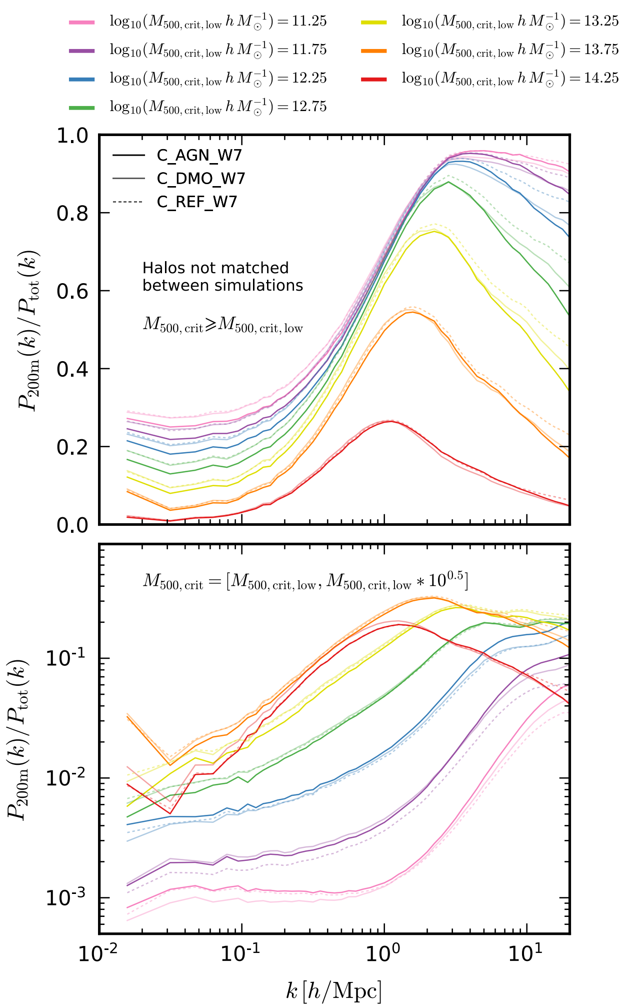

Figure 3. The halo clustering contribution as a function of mass, relative to the full power spectrum, for C_AGN_W7 (solid), C_DMO_W7 (transparent) and C_REF_W7 (transparent and dashed), at $z = 0$. The legend and particle selections are the same as in Fig. 2. The contribution of haloes with $M_{500,\,\mathrm{crit}} = 10^{14\pm0.25}\,\mathrm{M}_\odot/h$ to the full spectrum exceeds the contributions of haloes with other masses for $k < 3\,h\,\mathrm{Mpc}^{-1}$. AGN feedback lowers the fraction of mass residing in massive haloes ($M_{500,\,\mathrm{crit}} \gtrsim 10^{13}\,\mathrm{M}_\odot/h$), as well as the contribution to the full power spectrum on small scales $k \gtrsim 8\,h\,\mathrm{Mpc}^{-1}$ of haloes with $M_{500,\,\mathrm{crit}} \gtrsim 10^{11.75}\,\mathrm{M}_\odot/h$, though resolution effects start to play a significant role at this scale.

transition happens around the mass when AGN feedback becomes important, supporting the statement that AGN feedback is the cause. Comparing the bottom to the top panel, we see that C_AGN_W7 lies below C_DMO_W7 when all haloes are taken into account, showing again that what happens to clustering in the groups and clusters dominates the effect on the overall power.

To better compare the relative contributions of haloes between the different simulations, it is useful to consider ratios of power spectra instead. In Fig. 3, each of the lines portrayed in Fig. 2 is divided by the full power spectrum of the accompanying simulation to illustrate the contribution to the full spectrum for each halo mass bin. The masses and line styles (indicating simulations) are as in Fig. 2. Here, we still take $r_{200,\mathrm{m}}$ as the halo boundary.

On large scales, the contribution of haloes to the power flattens off to a fraction of ≈0.3 (depending on simulation) when all haloes are taken into account (pink lines). In this regime, the 2-halo term dominates: the overdensities are determined by the positions and masses/sizes of the haloes, the clustering in the interior of haloes has a negligible contribution. As we move to higher k (smaller scales), there is a massive rise in contribution around the scales that haloes are entered, which of course differs per mass bin. Along this rise, the 1-halo term starts to dominate over the 2-halo term, as most of the power comes from clustering in the interior of the haloes. Once the halo is entered, a maximum power contribution to the total is reached, after which it declines again for smaller scales. Note that for $k > 8\,h\,\mathrm{Mpc}^{-1}$ resolution effects start to influence the results noticeably, lowering the power. When all haloes are taken into account (pink line, top panel of Fig. 3), the contribution to the full power spectrum reaches >0.9 at $k \approx 3\,h\,\mathrm{Mpc}^{-1}$. The remaining percentage of power is provided by a combination of the cross-power between non-halo and halo particles and the autopower in non-halo particles (as seen in subsection 3.6).

The bottom panel of Fig. 3 shows the individual contributions of each halo mass bin to the full power spectra of C_AGN_W7, C_REF_W7, and C_DMO_W7. This panel clearly shows that the $10^{14\pm0.25}\,\mathrm{M}_\odot/h$ haloes contribute most to the full power spectrum for $k < 3\,h\,\mathrm{Mpc}^{-1}$, and lower mass bins take over on smaller scales. Note that resolution effects play some role in this, which generally lower the power on small scales ($k \gtrsim 8\,h\,\mathrm{Mpc}^{-1}$).

On large scales, the fraction of the total mass selected, when selecting the haloes in a certain mass bin, determines the fraction of power to the full power spectrum. As the selection is purely based on halo mass, one might expect all three simulations to lie on top of each other. However, because these are not the same haloes, this is not the case; the discrepancies become larger, as more haloes are taken into account (top panel, $k \sim 0.02\,h\,\mathrm{Mpc}^{-1}$). While C_REF_W7 and C_DMO_W7 are in quite good agreement, the total halo contribution on large scales is significantly lower in C_AGN_W7, as more mass is removed from haloes. Looking at the peak in contribution (when entering the halo) in the top panel of Fig. 3 for masses around $10^{13.75}\,\mathrm{M}_\odot/h$ (yellow and orange lines), there is a clear horizontal displacement between the power contribution of haloes to the full power spectrum in the C_AGN_W7 and C_DMO_W7. This is counterintuitive, since AGN feedback lowers the halo mass, effectively placing the more extended, denser haloes in a lower mass bin, from which one would expect the peak in C_AGN_W7 to move to larger scales (smaller k). Looking at the bottom panel, however, we see that the shift does not occur in individual halo mass bins, but is a cumulative effect of feedback reducing the halo mass by different amounts on different mass scales.

We also see that the peak of these haloes in C_REF_W7 is considerably higher than both other simulations, likely due to extra cross-power between halo particles and the large number of stars that have formed due to overcooling.

When comparing the C_AGN_W7, C_REF_W7, and C_DMO_W7 lines in Fig. 3, drawing conclusions is not straightforward because the haloes are not matched between simulations. Baryon cooling strongly peaks the density distribution towards the centre of the haloes, changing SO radii and thus the scale at which the halo is entered. Additionally, the removal of mass due to feedback also changes the profiles and therefore the 1-halo contribution, while also lowering the overall power of the haloes and shifting haloes between mass bins. To be able to better distinguish these different effects, in the remainder of Section 3 we will consider the relative contributions for matched catalogues of haloes.

Downloaded from https://academic.oup.com/mnras/article/528/3/4623/7590824 by Jacob Heeren user on 07 February 2025

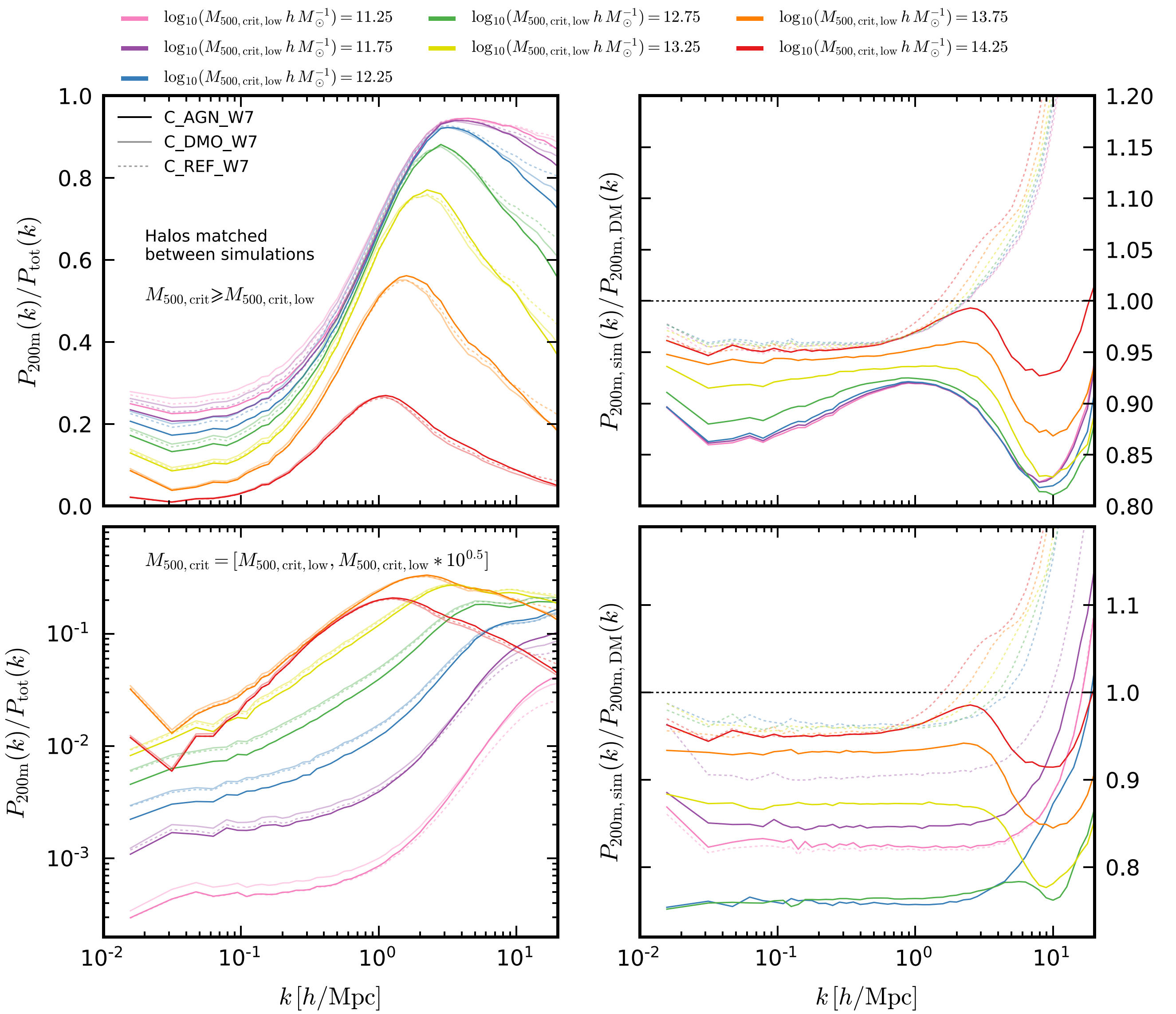

Figure 4. The left side of the figure is as in Fig. 3, except that the haloes are matched between C_DMO_W7 and the baryonic simulations. Only matched pairs are shown. The right side of the figure shows the power spectra of the C_AGN_W7 (solid) and C_REF_W7 (transparent and dashed) simulations divided by the power spectra of C_DMO_W7, for each halo mass bin. $M_{500,\,\mathrm{crit}}$ masses are measured in C_DMO_W7. AGN feedback lowers the masses of all haloes. On small scales, AGN feedback causes a dip in the C_AGN_W7/C_DMO_W7 power ratios of massive ($M_{500,\,\mathrm{crit}} \geq 10^{12.75}\,\mathrm{M}_\odot/h$) haloes, whereas the lower-mass haloes shown a sharp rise, like all C_REF_W7/C_DMO_W7 power ratios.

3.2 Autopower contributions for matched haloes

This section, discussing Fig. 4, compares the cosmo-OWLS simulations, C_DMO_W7, C_REF_W7, and C_AGN_W7, by matching the haloes between the simulations. The left side of Fig. 4 shows the power contribution to the full power spectrum for the same mass selections of haloes as in Fig. 3, but for a matched set of haloes. The right side shows the ratios between the power spectra of the baryon and DMO simulations (C_AGN_W7/C_DMO_W7, solid continuous, and C_REF_W7/C_DMO_W7, dashed transparent line style) for each mass bin, to illustrate the effect of baryons on the power in haloes for a range of halo masses.

On large scales, small k, the power contribution to the full power spectrum reflects the mass fraction of the selected haloes. Therefore, the top-left panel shows that the masses of the haloes are not the same in the two simulations. When taking only the largest haloes into account ($M_{500,\,\mathrm{crit}} \geq 10^{14.25}\,\mathrm{M}_\odot/h$, red lines), the masses in the baryon simulations are closest to those in C_DMO_W7, as seen in the top-right panel at $k \approx 0.02\,h\,\mathrm{Mpc}^{-1}$, where the power ratio C_AGN_W7/C_DMO_W7 ≈0.96. These haloes have such a deep potential well that AGN feedback is damped and does not have a substantial effect. As more lower-mass haloes are added to the sample, the power ratio between simulations lowers until it saturates at ≈0.88 for $M_{500,\,\mathrm{crit}} \geq 10^{12.25}\,\mathrm{M}_\odot/h$, where the bottom-right panel shows that haloes with masses lower than $10^{12.75}\,\mathrm{M}_\odot/h$ either have a similar or a higher C_AGN_W7/C_DMO_W7 ratio and the bottom-left panel shows that these mass bins have a much lower contribution to the full power spectrum than the more massive haloes. Consequentially, the C_AGN_W7/C_DMO_W7 ratios of the mass bins that take lower mass haloes into account as well as higher mass

Downloaded from https://academic.oup.com/mnras/article/528/3/4623/7590824 by Jacob Heeren user on 07 February 2025

ones, are determined by the C_AGN_W7/C_DMO_W7 ratios of the higher mass haloes up to $\sim 10^{14}\,\mathrm{M}_{\odot}/h$ and thus lowered by the AGN feedback processes these are subject to.

A possible reason why the simulation ratios of low-mass haloes, e.g. $10^{12\pm0.25}\,\mathrm{M}_{\odot}/h$ (solid purple line, Fig. 4), in the bottom-right panel are lower for AGN than REF, could be that these haloes are still indirectly effected by AGN feedback. Lower-mass haloes tend to cluster around high-mass ones, forming large groups. The powerful shock waves caused by AGN in massive haloes can carry out to far beyond these haloes, affecting all the other haloes in the vicinity. This might cause the haloes to lose all their gas due to a shock wave, or in milder cases, the expansion of the central halo weakens its gravitational pull making surrounding objects less strongly bound/expand. A more likely explanation is that the formation and evolution of the haloes were influenced by the AGN at an earlier stage. The gas around galaxies with AGN is much hotter, hindering the accretion and growth of smaller haloes and galaxies. However, this has not been verified in this research. Either way, the effects of AGN feedback are felt by lower-mass galaxies, as can be seen when comparing the solid (C_AGN_W7/C_DMO_W7) and transparent dashed (C_REF_W7/C_DMO_W7) lines in the bottom-right panel of Fig. 4. Note that the C_REF_W7/C_DMO_W7 ratio is also <1, due to gas pressure which impedes collapse. For low-mass haloes, $M_{500,\,\mathrm{crit}} < 10^{11.75}\,\mathrm{M}_{\odot}/h$, there are few particles making up the halo in these simulations, allowing small discrepancies to have a large influence on the power. We also note that van Daalen & Schaye (2015) found that such haloes are underrepresented at this resolution.

At k of a few, the power spectrum is almost completely determined by the clustering of matter inside haloes, as can be seen by the peak in the top-left panel of Fig. 4. Although the figure exhibits the same general shapes as the version without matching (Fig. 3), considering matched rather than mass-selected catalogues has significant effects. The different simulations meet at a point, just before the peak, when the halo is entered; this is expected as they are the same haloes, although this would cease to happen if larger amounts of mass were removed. Right after this point, the contribution of haloes to the power in C_AGN_W7 rises above that of C_DMO_W7 and C_REF_W7. This however does not mean that halo matter in the C_AGN_W7 simulation clusters most strongly on this scale, compared to the other simulations: in fact, the opposite is true. This effect comes from the differences in the full power spectra (through which we are dividing on the left-hand side of the figure), as is verified in the top-right panel of Fig. 4. Here we see that the power ratio between C_AGN_W7 and C_DMO_W7 (solid lines) is below unity for every mass bin. It is therefore likely the cross-power between matter around haloes and haloes themselves being decreased by the presence of AGN which causes the rise of the peak seen for C_AGN_W7 in the top-left panel, due to the AGN removing mass from the haloes and depositing it on larger scales, where it clusters less strongly.

Still keeping our focus on the top-right panel, we see that, as expected, the relative autopower contributions of haloes in different mass ranges compared to C_DMO_W7 is lower for C_AGN_W7 than for C_REF_W7, and that this difference is driven on large scales by the mass difference of $\sim 10^{12.5}\,\mathrm{M}_{\odot}/h$-$10^{14}\,\mathrm{M}_{\odot}/h$ haloes between these simulations. On small scales (at $k \geq 3\,h\,\mathrm{Mpc}^{-1}$), where the change in autopower is a reflection of the change in halo profile, the top-right panel shows a dip for all halo masses in the C_AGN_W7/C_DMO_W7 ratio. The C_REF_W7/C_DMO_W7 ratio rises above 1 at this scale because the dark matter haloes contract, reacting to the heavily clustered galaxy, and there is no AGN feedback to counter the contraction (the SN feedback being too weak to counter the contraction on the most relevant mass scales).

At $3 < k < 10\,h\,\mathrm{Mpc}^{-1}$, the C_AGN_W7/C_DMO_W7 power ratio for $M_{500,\,\mathrm{crit}} \geq 10^{12.75}\,\mathrm{M}_{\odot}/h$ haloes drops by $\approx$0.1, because of AGN feedback. At $k \geq 10\,h\,\mathrm{Mpc}^{-1}$, this ratio starts to rise again for all mass bins in the top-right panel, until, at $k = 20\,h\,\mathrm{Mpc}^{-1}$ each reaches more or less the value it had at $k \approx 3\,h\,\mathrm{Mpc}^{-1}$. This rise can be attributed to the reaction of dark matter to the behaviour of baryons at small (galaxy) scales ($k \sim 100\,h\,\mathrm{Mpc}^{-1}$), which cluster and increase the power, causing a contraction in the dark matter at larger scales ($k \sim 20\,h\,\mathrm{Mpc}^{-1}$), meaning the AGN effectively change clustering the most at intermediate scales inside haloes, relative to DMO. Despite their low contribution to the full power spectrum (bottom-left panel), the lower mass haloes have a part to play in the rise at $k \gtrsim 10\,h\,\mathrm{Mpc}^{-1}$, shown by the steeper slope of the C_AGN_W7/C_DMO_W7 power ratios at these scales in the top-right panel for the lines that take the lower-mass haloes into account. The behaviour of the lower mass galaxies ($M_{500,\,\mathrm{crit}} < 10^{12.75}\,\mathrm{M}_{\odot}/h$) can be explained by their lack of, but vicinity to, galaxies with AGN feedback: they are not affected internally, since they do not host AGN themselves, but their masses are lower than they would have been in a universe without AGN. The solid C_AGN_W7/C_DMO_W7 ratios in the bottom-right panel follow the same general shapes and have similar slopes as the transparent dashed ones (C_REF_W7/C_DMO_W7), albeit shifted horizontally, indicating similar physical effects.

We note that resolution effects, coming from the limited number of particles making up a halo, which prohibit measuring the clustering on very small scales and start to play a role at $k \gtrsim 8\,h\,\mathrm{Mpc}^{-1}$, lowering the power relative to a higher resolution simulation. This affects the DMO haloes in cosmo-OWLS most strongly, as these were run with half as many particles as the baryonic simulations, and therefore may affect the ratios shown here. However, the BAHAMAS simulation project uses 2-fluid simulations for DMO, so this effect is compensated (see subsection 2.1.1). As we will see in subsection 3.5, Fig. 7 shows that the ratios still exhibit the dip and rise for the BAHAMAS simulations, albeit somewhat differently, confirming that resolution effects are not the leading cause of the small-scale effects presented here.

3.3 Varying the SO regions

We now consider how the halo contributions depend on the choice of halo boundary. For simplicity we choose to only compare two simulations from the cosmo-OWLS simulations, DMO and the most realistic baryon simulation: C_DMO_W7 and C_AGN_W7. Fig. 5 is similar to Fig. 4 for C_AGN_W7 (solid) and C_DMO_W7 (transparent), but dashed lines now show the results for a $r_{500,\mathrm{c}}$ cut-off radius (dashed) compared to $r_{200,\mathrm{m}}$ (continuous). The mass selections are as in Fig. 4 and the haloes are matched between the simulations.

The most drastic effect of the change in the SO radius from $r_{200,\mathrm{m}}$ to $r_{500,\mathrm{c}}$ on the relative halo contribution to the total power spectrum (top-left panel of Fig. 5) is a horizontal shift of the peaks towards larger k. The $r_{500,\mathrm{c}}$ spherical overdensity region has a smaller radius than $r_{200,\mathrm{m}}$ and is often used to explore halo properties through X-ray observations. Direct or indirect effects from baryons are often more apparent when considering this region. Since the peak indicates the scale at which the halo is entered, the shift seen here is expected.

Furthermore, on large scales the power contribution to the full power spectrum is lower for $r_{500,\mathrm{c}}$, as less of the mass is taken into account in these calculations. Still, taking C_DMO_W7 as an

Downloaded from https://academic.oup.com/mnras/article/528/3/4623/7590824 by Jacob Heeren user on 07 February 2025

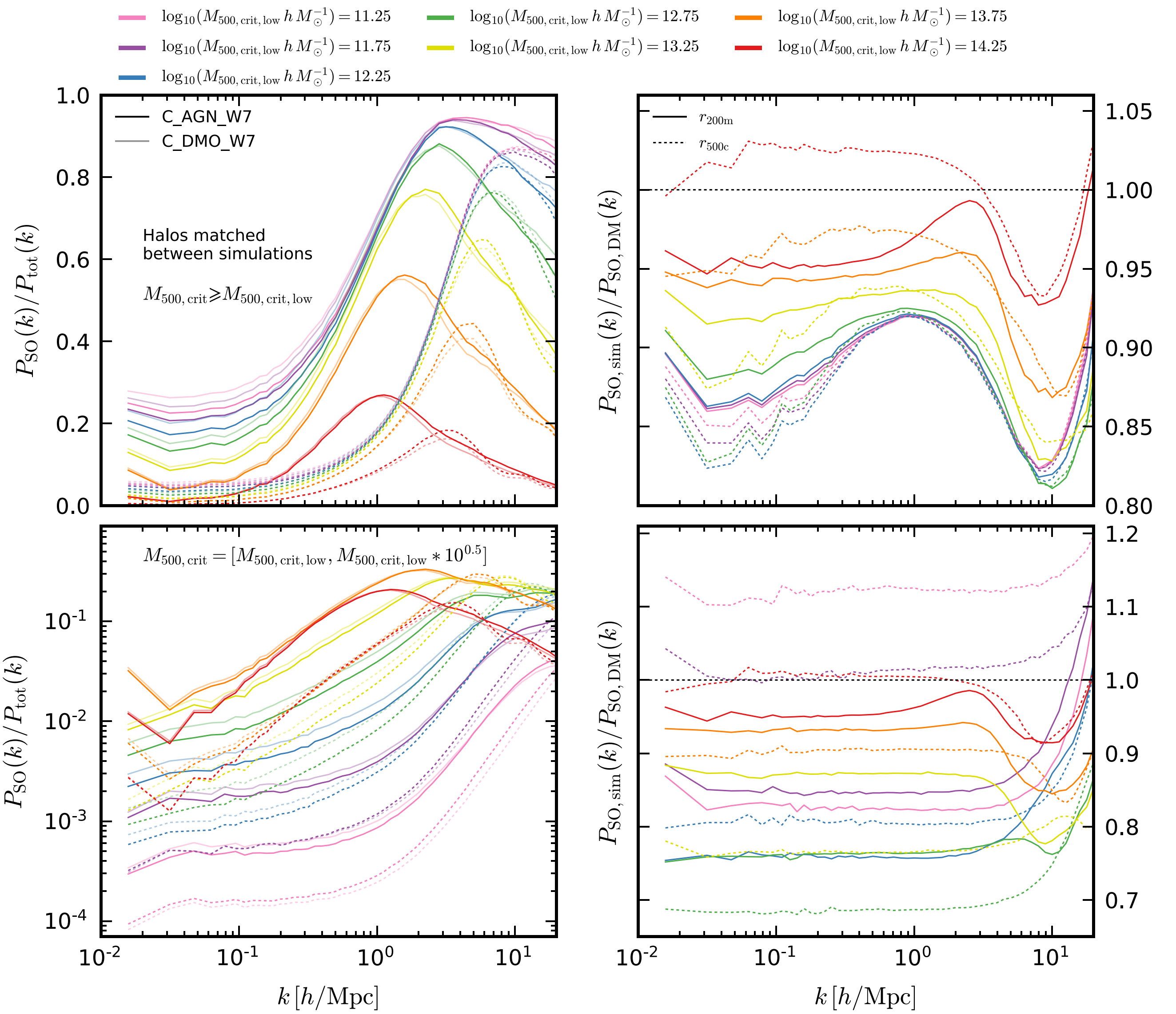

Figure 5. Absolute and relative halo power contributions for C_AGN_W7 and C_DMO_W7 as in Fig. 4, but dashed lines now show the results when only particles within $r_{500,\mathrm{c}}$ are included. The peak in halo power contribution is moved to higher k for particles within $r_{500,\mathrm{c}}$, relative to the results for $r_{200,\mathrm{m}}$. Although much less mass is included in the smaller $r_{500,\mathrm{c}}$ regions, the power on small scales only drops slightly, as they are highly biased. As the bottom-left panel shows, for both SO regions $\sim 10^{14}\,\mathrm{M}_\odot/h$ haloes provide the largest contribution to the total power up to $k\sim$ a few. From the bottom-right panel, we see that for group-sized haloes the effects of AGN feedback are more extensive within $r_{500,\mathrm{c}}$, compared to within $r_{200,\mathrm{m}}$.

example, the particles within $r_{500,\mathrm{c}}$ of haloes contribute a maximum fraction of $\approx$0.89 of the full power through their autopower alone, while the particles within $r_{200,\mathrm{m}}$ reach $\approx$0.96 of the full power. In contrast, on large scales, $k\sim 0.02\,h\,\mathrm{Mpc}^{-1}$, these SO regions account $\approx$0.06 of the total for $r_{500,\mathrm{c}}$ and for $\approx$0.29 of the total for $r_{200,\mathrm{m}}$. Since the difference in power between SO regions on the largest scales is just a reflection of their relative total mass fractions, this indicates that the $r_{500,\mathrm{c}}$ regions contain slightly less than half the mass of the $r_{200,\mathrm{m}}$ regions. We thus see that almost all power on small scales comes from clustering within the $r_{500,\mathrm{c}}$ regions of haloes, even though these regions include much less mass.

The bottom-left panel of Fig. 5 shows that for both SO radii, the $10^{14\pm0.25}\,\mathrm{M}_\odot/h$ haloes provide the largest contribution to the full power spectrum for $k\lesssim 3\,h\,\mathrm{Mpc}^{-1}$, although the dominance of these haloes continues up to $k\sim 7\,h\,\mathrm{Mpc}^{-1}$ for particles within $r_{500,\mathrm{c}}$.

On scales that are inside the halo ($k > k_{\mathrm{peak}}$), the $r_{500,\mathrm{c}}$ halo power spectra exhibit a slight oscillation that is caused by the sharp boundary of $r_{500,\mathrm{c}}$, particularly in the bottom panel. This is roughly equivalent to the oscillations seen in the Fourier transform of a top-hat filter, and only more apparent for $r_{500,\mathrm{c}}$ than for $r_{200,\mathrm{m}}$ due to the higher density at the cut-off radius, and is therefore not a physical effect.

Comparing C_AGN_W7 and C_DMO_W7 in the top-left panel of Fig. 5, we see that the differences in halo contributions are larger around the peak for $r_{500,\mathrm{c}}$ than for $r_{200,\mathrm{m}}$. Specifically, when baryons and AGN are included the peak autopower contribution of haloes to the power spectrum is increased – however, the top-right panel shows that this is again due to the total power

Downloaded from https://academic.oup.com/mnras/article/528/3/4623/7590824 by Jacob Heeren user on 07 February 2025

spectrum decreasing in AGN relative to DMO, rather than the halo power itself. Like in subsection 3.2, we thus conclude that the increase in the relative peak power contributions are due to a decrease in cross-power of haloes with the matter around it. We consider the role of the cross-power further in subsection 3.6 and Section 4.

Comparing the $r_{200,\mathrm{m}}$ and $r_{500,\mathrm{c}}$ results in the top-right panel further, we also see that the 'bump' seen around $k \approx 3\,h\,\mathrm{Mpc}^{-1}$ for $r_{200,\mathrm{m}}$ for the two most massive halo mass bins (red and orange lines) is not seen for $r_{500,\mathrm{c}}$. This bump is due to the mass moved to the outskirts of the halo by AGN feedback, and the fact that it is not visible for $r_{500,\mathrm{c}}$ means that a significant fraction of the mass is being deposited between $r_{500,\mathrm{c}}$ and $r_{200,\mathrm{m}}$ in the most massive haloes. The bottom-left panel shows that this is mostly due to the contribution of the very most massive haloes probed here (red line). At the same time, from the same panel we see that the $\sim 10^{14.5}\,\mathrm{M}_\odot/h$ haloes show a higher C_AGN_W7/C_DMO_W7 ratio for particles within $r_{500,\mathrm{c}}$ than particles within $r_{200,\mathrm{m}}$ on large scales, around unity for $k \lesssim 3\,h\,\mathrm{Mpc}^{-1}$. This indicates that the mass added to $r_{500,\mathrm{c}}$ by the cooling of baryons is balanced by the mass ejected to $r > r_{500,\mathrm{c}}$ by AGN feedback for these haloes – keeping in mind that the sizes of these regions may have changed between these simulations as well (see subsection 3.4). We will refer to the region between $r_{500,\mathrm{c}}$ and $r_{200,\mathrm{m}}$ as the halo annulus, and consider it again in subsection 4.2.

Looking at the other halo mass bins shown in the bottom-right panel of Fig. 5, we see that for $M_{500,\,\mathrm{crit}} \geq 10^{12.75}\,\mathrm{M}_\odot/h$ (green, yellow and orange lines), the C_AGN_W7/C_DMO_W7 ratios are much lower for $r_{500,\mathrm{c}}$ than for $r_{200,\mathrm{m}}$. This is expected, as mass is removed from the central regions by AGN feedback and deposited on larger scales, thereby affecting the mass within $r_{500,\mathrm{c}}$ more than that within $r_{200,\mathrm{m}}$. Contrarily, for $10^{12.5\pm0.25}\,\mathrm{M}_\odot/h$ haloes (blue), the C_AGN_W7/C_DMO_W7 ratio for $r_{500,\mathrm{c}}$ lies above that for $r_{200,\mathrm{m}}$, but is still below unity indicating that the entire halo is less massive due to impeded growth or stripping of gas, as mentioned previously, and most of the mass is taken from/not added to the outer region of the halo. For even less massive haloes (pink and purple lines), the C_AGN_W7/C_DMO_W7 ratio even exceeds unity for $r_{500,\mathrm{c}}$, indicating that the cooling of baryons dominates over their ejection.

Note that the SO radii change between the simulations as the halo mass changes, limiting the conclusions that can be drawn from this figure concerning where mass is deposited. In subsection 3.4, the radius is kept constant between simulations, to investigate this in more depth.

Finally, we note that the halo autopower ratios between C_AGN_W7 and C_DMO_W7 for all mass bins as shown in the bottom-right panel of Fig. 5 are very nearly constant on large scales. For $r_{500,\mathrm{c}}$, this even extends up to $k \sim$ a few or beyond, depending on halo mass. This indicates that the removal of mass from this region to great approximation determines the change in clustering of these haloes, irrespective of any changes in halo profiles, and that scale-dependent changes in halo clustering (such as seen in the top panels) are simply a consequence of combining different halo mass bins. As we will see in subsection 3.4, this remains true when keeping the SO radius fixed. This suggests that one could accurately predict the total power suppression due to feedback by only knowing the fraction of mass that was removed from certain clustered regions. Based on this, we develop a model to do just that in Section 4.

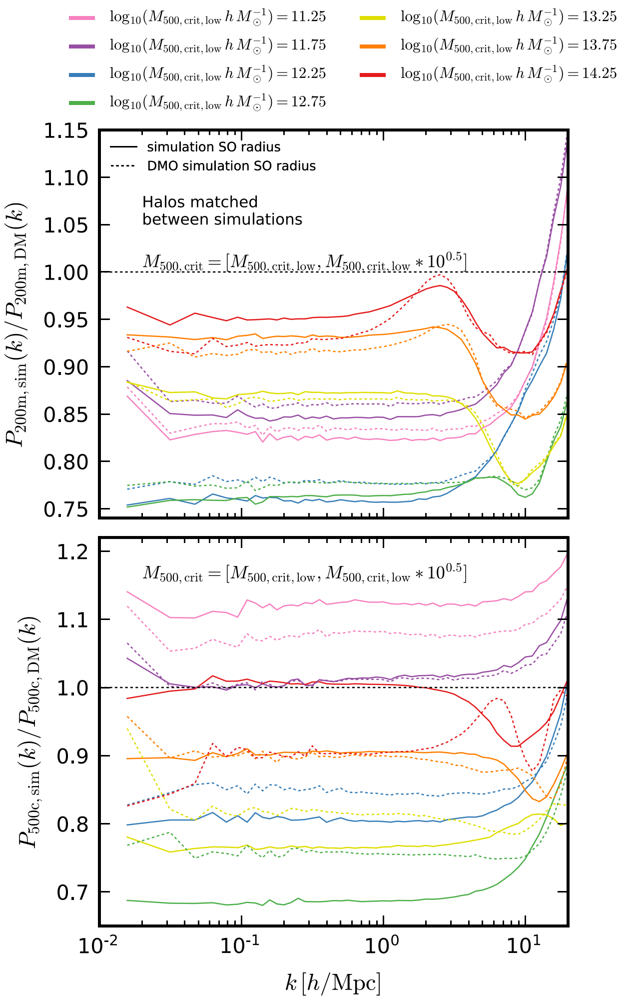

Figure 6. Similar to the bottom-right panel of Fig. 5, with results for $r_{200,\mathrm{m}}$ shown in the top panel and those for $r_{500,\mathrm{c}}$ in the bottom panel, but now with two definitions for the SO radii: either the particle selection criterion is as before, that is, using the SO radius measured in each simulation (continuous linestyle), or the SO radius as measured in C_DMO_W7 is used for C_AGN_W7 as well (dashed linestyle). The change in SO radius between C_AGN_W7 and C_DMO_W7 varies between $r_{200,\mathrm{m}}$ and $r_{500,\mathrm{c}}$ and with halo mass, with the $r_{500,\mathrm{c}}$ result being most strongly affected.

3.4 Keeping the SO radius fixed between simulations

To get a sense of the how much matter is ejected from which radius by AGN feedback and where it is deposited, not only do the haloes need to be matched, but a constant halo boundary (SO radius) needs to be taken between simulations, which are limited to cosmo-OWLs simulations C_DMO_W7 and C_AGN_W7 in this section. This way, the comparison between simulations can be taken one step further, as not only processes within (or outside of) the same haloes, but also within certain regions of space in these haloes can be considered.

In Fig. 6, the C_AGN_W7/C_DMO_W7 power ratio is displayed for the usual range in halo masses, for a particle selection where either the simulation SO radius ($r_{200,\mathrm{m}}$, continuous lines), or C_DMO_W7 SO radius (dashed lines) marks the halo boundary.

Although there are slight changes in the ratio between C_AGN_W7 and C_DMO_W7 power spectra for the $r_{200,\mathrm{m}}$ simulation radii and the

Downloaded from https://academic.oup.com/mnras/article/528/3/4623/7590824 by Jacob Heeren user on 07 February 2025

C_DMO_W7 $r_{200,\mathrm{m}}$ radii, the C_AGN_W7/C_DMO_W7 power ratios of the two regions mostly follow the same trends and have the same shapes (top panel). On large scales, a comparison of the lines tells us that there is less mass in C_AGN_W7 haloes within the C_DMO_W7 $r_{200,\mathrm{m}}$ radius than in the C_AGN_W7 SO radius for massive haloes ($M_{500,\,\mathrm{crit}} \gtrsim 10^{13.25}\,\mathrm{M}_\odot/h$), indicating that the C_DMO_W7 SO radius is smaller. The C_AGN_W7 $r_{200,\mathrm{m}}$ has increased compared to the C_DMO_W7 $r_{200,\mathrm{m}}$ because mass has been ejected from inside this radius to outside it, causing the density profile of the haloes to flatten in C_AGN_W7.

For lower-mass haloes ($M_{500,\,\mathrm{crit}} \leq 10^{13.25}\,\mathrm{M}_\odot/h$), the higher C_AGN_W7/C_DMO_W7 ratios for the C_DMO_W7 SO radius at $k \sim 0.02\,h\,\mathrm{Mpc}^{-1}$ indicate that there is more mass in the C_DMO_W7 $r_{200,\mathrm{m}}$ than in the C_AGN_W7 $r_{200,\mathrm{m}}$ in C_AGN_W7, implying a larger C_DMO_W7 $r_{200,\mathrm{m}}$.

The bottom panel of Fig. 6 shows the same as the top panel, except that the halo boundary SO radii are the C_DMO_W7 and simulation $r_{500,\mathrm{c}}$. At this radius, the consequences of changing the radius to the C_DMO_W7 SO radius have much more impact. Interestingly enough, only haloes with $10^{12.25} \lesssim M_{500,\,\mathrm{crit}} \lesssim 10^{13.75}\,\mathrm{M}_\odot/h$ (blue, green, and yellow lines) have an increased C_AGN_W7/C_DMO_W7 power ratio for the C_DMO_W7 $r_{500,\mathrm{c}}$, when compared to the simulation $r_{500,\mathrm{c}}$ power ratio, on large scales. The nearest mass bins in both directions (purple and orange lines) suggest no change in C_AGN_W7/C_DMO_W7 ratio on large scales and the lowest ($10^{11.5\pm0.25}\,\mathrm{M}_\odot/h$, pink) and highest ($10^{14.5\pm0.25}\,\mathrm{M}_\odot/h$, red) mass haloes have lower C_AGN_W7/C_DMO_W7 ratios when choosing the C_DMO_W7 $r_{500,\mathrm{c}}$ instead of the simulation $r_{500,\mathrm{c}}$. This suggests that for intermediate-mass haloes, the C_DMO_W7 $r_{500,\mathrm{c}}$ is larger than the C_AGN_W7 $r_{500,\mathrm{c}}$; for the more massive or lower-mass haloes, the C_DMO_W7 $r_{500,\mathrm{c}}$ is smaller than or equal to the C_AGN_W7 $r_{500,\mathrm{c}}$. Therefore, the intermediate-mass haloes are dominated by mass ejection inside $r_{500,\mathrm{c}}$, while the lower-mass and more massive haloes are dominated by contraction.

The most significant change in the bottom panel is seen for the most massive haloes, where the choice of the simulation or DMO $r_{500,\mathrm{c}}$ radius not only shifts the contribution by 10 per cent vertically, but also shows either a large bump or large dip for $k \approx 7\,h\,\mathrm{Mpc}^{-1}$, depending. This suggests that the DMO $r_{500,\mathrm{c}}$ radius is both smaller than the C_AGN_W7 halo radius for these haloes, and simultaneously such that it captures a lot of the material pushed out by feedback. The $r_{500,\mathrm{c}}$ radius in the baryonic simulation, on the other hand, is large enough that the effect of this density bump is effectively smoothed out. To a lesser extent, this effect is also present in the top panel, where the height of the bump at $k \approx 3\,h\,\mathrm{Mpc}^{-1}$ is increased for the two most massive halo mass bins when the DMO $r_{200,\mathrm{m}}$ radius is used.

3.5 Varying the feedback temperature

In order to examine the role of the feedback strength qualitatively on the halo contributions for matched haloes, we can repeat our analysis for the three BAHAMAS simulations where the AGN heating temperature is varied: B_AGN_W9, B_AGNlow_W9, and B_AGNhigh_W9. The heating temperature is not an observational parameter, but a model parameter, which, together with the number of particles that are heated in a feedback event (n_{heat}), determines the strength of the AGN feedback (see subsection 2.1.1 for details about the AGN feedback model). Recall that in the fiducial BAHAMAS simulation, B_AGN_W9, the heating temperature has been calibrated to fit the hot gas fractions in groups and clusters. B_AGNlow_W9, which has less effective heating, therefore produces too little hot gas, while B_AGNhigh_W9, which has stronger heating, produces too much, compared to the average of the observations used by McCarthy et al. (2017). Fig. 7 shows the contribution of haloes to the full power spectrum (left side) and baryon-dark matter power ratios (right side) for matched sets of B_DMO_W9, B_AGN_W9, B_AGNlow_W9, and B_AGNhigh_W9, for the same range of halo mass bins as the previous figures. The AGN feedback temperature has a relatively large impact on the B_AGN_W9/B_DMO_W9 full power spectrum ratio for $k \gtrsim 0.1\,h\,\mathrm{Mpc}^{-1}$. However, the changes in the halo mass bin power spectra and the full matter spectra are of similar order, resulting in a relatively small impact of the AGN feedback temperature on the contribution of each halo mass bin to the full power spectrum as can be seen in the top-left and bottom-left panels of Fig. 7. The two sets of dashed lines show simulations with a lower (long dashed) or a higher (short dashed) heating temperature, and show only minor differences with respect to the calibrated feedback strength (solid continuous line).

On large scales, the discrepancies between the contributions to the full power spectrum of B_AGN_W9, B_AGNlow_W9, and B_AGNhigh_W9 are more substantial around $M_{500,\,\mathrm{crit}} \approx 10^{12.5-13}\,\mathrm{M}_\odot/h$ (bottom-left panel), suggesting that the masses of these haloes are most sensitive to changes in AGN feedback temperature (as confirmed by the bottom-right panel).

The top-right panel of Fig. 7 indicates that the effect of AGN feedback temperature on the power ratios between the AGN simulations and B_DMO_W9 is quite substantial. Although it is mostly a vertical displacement, where a higher feedback temperature results in a lower AGN/B_DMO_W9 ratio, there are some changes in AGN/B_DMO_W9 ratio shape as well. For the most massive haloes ($M_{500,\,\mathrm{crit}} \geq 10^{14.25}\,\mathrm{M}_\odot/h$, red line), the top and bottom-right panels show a clear change in AGN/B_DMO_W9 ratio slope at $k \sim 4\,h\,\mathrm{Mpc}^{-1}$, indicating a change in profile. The B_AGNlow_W9/B_DMO_W9 power ratio (low AGN feedback temperature) mimics the shapes of the C_AGN_W7/C_DMO_W7 power ratio, in the top-right panel of Fig. 4. This behaviour indicates that these haloes are hardly affected by the AGN feedback: it is damped so aggressively by their deep potential wells, the effects on the haloes are no longer dominating the shape of the B_AGNlow_W9/B_DMO_W9 power ratio. The B_AGNhigh_W9/B_DMO_W9 ratio (high AGN feedback temperature) for the most massive haloes ($M_{500,\,\mathrm{crit}} \geq 10^{14.25}\,\mathrm{M}_\odot/h$, red line) follows the slope of the other, less massive haloes. Apparently, at this temperature the potential wells of the haloes are no longer deep enough to produce a significant damping effect. The $10^{14\pm0.25}\,\mathrm{M}_\odot/h$ (orange lines) haloes exhibit a similar, albeit a reduced, effect, as illustrated by the top and bottom-right panels.

Finally, looking at the bottom-right panel, we see the same trends as before: increasing/decreasing the feedback temperature mainly lowers/raises the mass and therefore the relative autopower contribution at each halo mass, where the largest dependence on feedback temperature is seen around $\sim 10^{13}\,\mathrm{M}_\odot/h$. For the most massive haloes, an effect on the halo profile can also be seen.

3.6 Other contributions to the power spectrum

We have thus far only considered autopower spectra – that is, the clustering of haloes of a given mass relative to their own population. While the autopower spectrum of all halo particles above a given mass (the relative contribution of which was typically shown in the top panels of the preceding figures) provides the dominant contribution to the total power spectrum for $k \gtrsim 0.5\,h\,\mathrm{Mpc}^{-1}$, other significant contributions exist, in the form of the autopower spectrum of non-

Downloaded from https://academic.oup.com/mnras/article/528/3/4623/7590824 by Jacob Heeren user on 07 February 2025

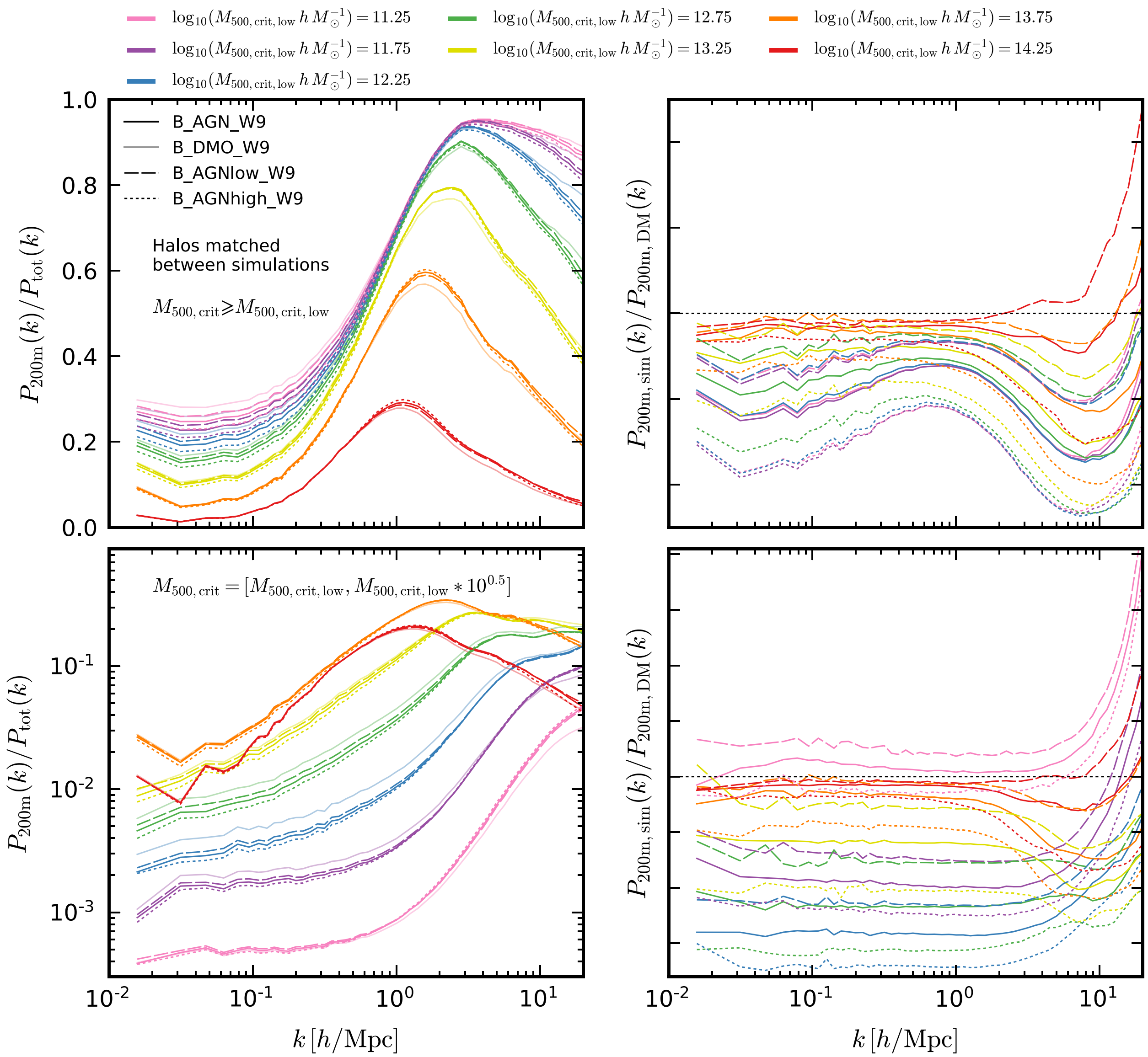

Figure 7. As Fig. 4, but showing results for BAHAMAS (B_AGN_W9, B_DMO_W9, B_AGNlow_W9, and B_AGNhigh_W9) rather than cosmo-OWLS. These simulations shown the change in impact of AGN feedback on haloes of different masses when the strength of the AGN feedback is varied (through the heating temperature). The heating temperature has a large influence on the C_AGN_W7/C_DMO_W7 ratios (right side), while the contribution of the halo mass bins to their corresponding full spectra remain similar.

halo particles (i.e. those that live outside of any particular overdensity region) and the cross-power spectrum of non-halo and halo particles. If we choose to separate the haloes into different mass bins, the number of auto- and cross-power terms contributing to the power spectrum sharply increases, as we need to add cross-spectra of particles in haloes of mass A with those in haloes of mass B (etc), and cross-spectra with non-halo particles for all mass bins. It is therefore more convenient (and useful) to instead consider the power spectrum as a sum of the cross-spectra of non-overlapping groups of particles – namely, haloes in some particular mass bin and non-halo particles – with all matter.

In Fig. 8, we show these cross-power terms for B_DMO_W9. To better separate halo from non-halo matter, here we again define haloes as $r_{200,\mathrm{m}}$ overdensity regions, but still select on their $M_{500,\,\mathrm{crit}}$ mass as before. The halo–matter cross terms are shown as coloured lines for different mass bins, with their total shown as solid grey. Adding the non-halo–matter cross term (where non-halo matter is defined here as all matter not in haloes $M_{500,\,\mathrm{crit}} > 10^{11.25}\,\mathrm{M}_\odot/h$), shown as dashed grey, yields exactly the total power spectrum (black). On large scales, the total halo and non-halo cross terms contribute almost equally to the total power spectrum, as they contain a comparable amount of mass. On small scales however, the halo cross term fully dominates, as expected. It should be noted that the division into halo and non-halo matter is a function of resolution, as with increased resolution we expect more diffuse matter to be resolved into low-mass haloes – however, with the current resolution we are already in a regime where the non-halo–matter cross term is subdominant on all scales.

In the following section, we show how we can exploit this division into cross terms to accurately model the power suppression in baryonic simulations.

Downloaded from https://academic.oup.com/mnras/article/528/3/4623/7590824 by Jacob Heeren user on 07 February 2025

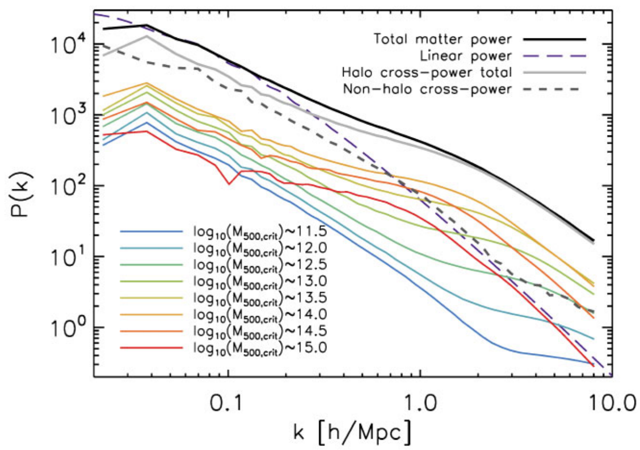

Figure 8. The power spectrum of B_DMO_W9 (solid black) and its halo (solid grey) and non-halo (dashed grey) cross-power components, $P_{\rm mh,\,200m}$ and $P_{\rm mnh,\,200m}$, respectively (see Section 4). The mass-weighted halo power in different mass bins, $f_{{\rm M},\,i,\,200{\rm m}}\,P_{{\rm mh},\,i,\,200{\rm m}}$, is shown as solid coloured lines. All haloes are selected on their $M_{500,\,\rm crit}$ mass. A linear power spectrum (long-dashed purple) is shown for comparison. The halo cross-power dominates on small scales, but on large scales halo and non-halo particles contribute roughly equally to the total power, as the total mass in both components is similar.

4 A 'RESUMMATION' MODEL FOR THE BARYONIC SUPPRESSION OF MATTER CLUSTERING

Let us call the cross-power of haloes in mass bin i and all matter, $P_{{\rm mh},\,i,\,\Delta}({\rm k})$. Here we will define haloes as regions with an overdensity Δ relative to the critical density $\rho_{\rm crit}$, for example $\Delta = 200\Omega_{\rm m}$ or $\Delta = 500$. Each halo mass bin will contain some fraction of the total mass in a volume, let us call these fractions $f_{{\rm M},\,i,\,\Delta}$.

We will refer to the matter–matter autopower spectrum as $P_{\rm mm}({\rm k})$. The halo cross terms are assumed to be un-normalized with respect to mass – the large-scale (linear) halo bias of haloes in mass bin i, then, is given by

$$b_{i,\Delta} = \lim_{k\to 0} \frac{P_{{\rm mh},i,\Delta}(k)}{P_{\rm mm}(k)}. \tag{2}$$

In practice, we will calculate the bias by averaging the power ratio on large scales ($k \lesssim 0.13\,h/{\rm Mpc}$), where it is roughly constant.

As discussed in subsection 3.6, we can write the matter autopower spectrum as a sum over all halo-matter cross terms, plus a cross term between all matter and the matter not in haloes. This necessarily includes matter in unresolved haloes. Since haloes are highly biased, this last cross term is expected to be dominated by matter just outside haloes (see also subsection 3.5). We will refer to the cross term of all matter with matter not in (resolved) haloes as $P_{\rm mnh,\,\Delta}(k)$ (note that this term, too, depends on our choice of overdensity region). By definition, then, these cross-power terms must satisfy

$$P_{\rm mm}(k) = P_{{\rm mnh},\Delta}(k) + \sum_i f_{{\rm M},i,\Delta}\, P_{{\rm mh},i,\Delta}(k), \tag{3}$$

where the sum is over all halo mass bins, and thus gives the total contribution of matter in (resolved) haloes.[3]

[3]Note that for consistency we could also have defined the matter–non-halo cross term as $(1 - \sum_i f_{{\rm M},\,i,\,\Delta}) P_{\rm mnh,\,\Delta}(k)$, but for the sake of brevity we have absorbed the mass fraction of non-halo matter into $P_{\rm mnh,\,\Delta}(k)$.

All quantities considered here can be readily calculated from DMO simulations. Fig. 8 shows these quantities for B_DMO_W9.

4.1 Accounting for mass-loss

Let us now consider what happens to these different terms as matter is redistributed by the processes associated with galaxy formation. While these processes change halo profiles – for example by gas cooling to small scales and forming stars, contracting the inner dark matter halo – the main effect on large scales is caused by removing mass from clustered regions. Therefore, on sufficiently large scales we can approximate the effects of galaxy formation by scaling the mass fractions of haloes by the mass they retained – that is, the ratio of the mass of a feedback-affected halo and its DMO equivalent.

Let us call the mean retained mass fraction for haloes in mass bin i, $f_{{\rm ret},\,i,\,\Delta}$. Let us further assume, just for the moment, that the total matter distribution we cross-correlate with is fixed to the DMO distribution. The total contribution to the matter–matter power spectrum of feedback-affected haloes then becomes

$$\begin{aligned} P'_{{\rm mh},\Delta}(k) &\equiv \sum_i f_{{\rm ret},i,\Delta}\, f_{{\rm M},i,\Delta}\, P_{{\rm mh},i,\Delta}(k) \\ &\equiv \sum_i f'_{{\rm M},i,\Delta}\, P_{{\rm mh},i,\Delta}(k), \end{aligned} \tag{4}$$

where the prime indicates a correction for retained mass.

The mass removed from haloes has to go somewhere, in such a way that the total mass in the volume is conserved. One option is to add this mass to a linear power component – however, the ejected mass is expected to stay around haloes, and therefore still cluster more significantly than linear. We thus add the mass to the non-halo component, which likely was already dominated by mass around haloes. One wrinkle is that we are removing mass from biased regions – we therefore need to take bias into account to ensure that the power at low k after modelling galaxy formation still converges to the original value. The ratio of the corrected non-halo cross-contribution to the original non-halo cross-contribution by definition satisfies

$$\begin{aligned} \frac{P'_{{\rm mnh},\Delta}(k)}{P_{{\rm mnh},\Delta}(k)} &= \frac{P'_{\rm mm}(k) - \sum_i f_{{\rm ret},i,\Delta} f_{{\rm M},i,\Delta} P_{{\rm mh},i,\Delta}(k)}{P_{\rm mm}(k) - \sum_i f_{{\rm M},i,\Delta} P_{{\rm mh},i,\Delta}(k)} \\ &= \frac{P'_{\rm mm}(k)/P_{\rm mm}(k) - \sum_i f'_{{\rm M},i,\Delta} P_{{\rm mh},i,\Delta}(k)/P_{\rm mm}(k)}{1 - \sum_i f_{{\rm M},i,\Delta} P_{{\rm mh},i,\Delta}(k)/P_{\rm mm}(k)}. \end{aligned} \tag{5}$$

If we now consider the low-k limit of this expression, and demand that $\lim_{k\to 0} P'_{\rm mm}(k)/P_{\rm mm}(k) = 1$, we find

$$\frac{P'_{{\rm mnh},\Delta}}{P_{{\rm mnh},\Delta}} = \frac{1 - \sum_i f_{{\rm ret},i,\Delta} f_{{\rm M},i,\Delta} b_{i,\Delta}}{1 - \sum_i f_{{\rm M},i,\Delta} b_{i,\Delta}}. \tag{6}$$

We thus see that to preserve the power on the largest scale when redistributing mass, we need to not just conserve mass, but the product of mass and bias.

Finally, we have to drop our temporary assumption that the total matter distribution we cross-correlate with is held fixed. Luckily, at this point we already know how the contributions from both the halo and non-halo matter distributions transform, and therefore how the total matter contribution transforms. Using double primes to indicate a correction for halo mass-loss in both matter components that make up the cross-power, we find

$$\frac{P''_{\rm mm}}{P_{\rm mm}} = \left(\frac{P'_{\rm mm}}{P_{\rm mm}}\right)^2 \equiv q_\Delta^2. \tag{7}$$

The doubly corrected halo-matter cross-power term then becomes $P''_{{\rm mh},\Delta} = q_\Delta P'_{{\rm mh},\Delta}$, and similarly $P''_{{\rm mnh},\Delta} = q_\Delta P'_{{\rm mnh},\Delta}$.

Downloaded from https://academic.oup.com/mnras/article/528/3/4623/7590824 by Jacob Heeren user on 07 February 2025

In summary, this model takes DMO halo mass fractions, linear biases and (cross-)power spectra, and combines them with the mean fraction of mass retained by haloes that have undergone galaxy formation, relative to their DMO equivalent, to predict the change in the total power spectrum. This mean fraction of mass retained, $f_{\mathrm{ret},\,i,\,\Delta}$, can be calculated as the total mass ratio of (matched) haloes in a hydrodynamical simulation and its DMO equivalent. Observationally, $f_{\mathrm{ret},\,i,\,\Delta}$ can in principle be derived from the mean observed baryon fractions of haloes of a certain mass, $\bar{f}_{\mathrm{b},i,\Delta}$, relative to the cosmic baryon fraction. Specifically, under the assumption that all matter removed from the halo was baryonic matter, one would find the retained fraction to be

$$f_{\mathrm{bc},i,\Delta} \equiv \frac{1 - \Omega_{\mathrm{b}}/\Omega_{\mathrm{m}}}{1 - \bar{f}_{\mathrm{b},i,\Delta}}, \tag{8}$$

where $\bar{f}_{\mathrm{b},i,\Delta} = M_{\mathrm{bar},i}/M_{\mathrm{tot},i}$ is the mean baryon fraction measured in haloes in mass bin i. This can be straightforwardly derived assuming that the 'original' baryon fraction of each halo is $\Omega_{\mathrm{b}}/\Omega_{\mathrm{m}}$, and that the retained CDM fraction, equal to $f_{\mathrm{ret},\,i,\,\Delta}/f_{\mathrm{bc},\,i,\,\Delta}$, is unity.

However, in reality the dark matter will respond gravitationally to the loss of mass, and additional mass will be lost as the halo relaxes. The amount of additional mass lost as a consequence of relaxation after a baryonic ejection event will be explored in Wolfs & van Daalen (in preparation). For now, we note that the following linear relation is accurate to $\lesssim 1$ per cent on average for haloes $M_{\mathrm{h},i,500\mathrm{c}} \gtrsim 10^{12.5}\,\mathrm{M}_{\odot}/h$ in all cosmo-OWLS and BAHAMAS simulations explored here, regardless of variations in cosmology or feedback strength

$$f_{\mathrm{ret},i,\Delta} \approx a(f_{\mathrm{bc},i,\Delta} - b), \tag{9}$$

with $a \approx 1.768$ and $b \approx 0.4206$ for $\Delta = 200\Omega_{\mathrm{m}}$. For $\Delta = 500$, the best fit coefficients are $a \approx 2.311$ and $b \approx 0.5251$, though we note that for this overdensity radius the variance is significantly larger (rms ≈ 2 per cent).[4] Crucially, this relation links the baryon fraction measured at a retained total mass (which is what we observe) to a retained fraction at a DMO total mass – hence no shifting of mass bins is necessary in applying this relationship to equations (3)–(6).

For lower-mass haloes ($M_{\mathrm{h},i,500\mathrm{c}} \leq 10^{12}\,\mathrm{M}_{\odot}/h$), the baryon fraction is more challenging to measure observationally. After checking that these haloes play a negligible role in setting the power suppression up to $k \approx 10\,h\,\mathrm{Mpc}^{-1}$, we fix the retained fractions for these halo masses to unity.

4.2 Combining overdensity regions

In principle, we now have all the ingredients to apply this model in practice for a given choice of overdensity region, using the mean baryon fraction measured inside that region for different halo mass bins to re-scale and re-sum DMO cross-power spectra. But, if these measurements are available for multiple overdensity regions – which is now feasible through combinations of X-ray, thermal Sunyaev–Zel'dovich and optical/infrared observations – we can combine this information to model the power spectra more accurately. As we will show, doing so can greatly compensate for the approximation that the halo profiles are fixed.

Say that we measure the total (retained) mass and baryon fraction of a sample of haloes for both $\Delta = 500$ and $\Delta = 200\Omega_{\mathrm{m}}$. We can then calculate the retained fraction for each region with equation (9). The net fraction of the 'original' DMO mass that has been removed from $r_{500,\mathrm{c}}$, but not $r_{200,\mathrm{m}}$, is then $f_{\mathrm{ret},\,i,\,200\mathrm{m}} - f_{\mathrm{ret},\,i,\,500\mathrm{c}}$. As shown in subsection 3.3, this fraction is quite significant for massive haloes. We will once more refer to the region $r_{500,\mathrm{c}} < r < r_{200,\mathrm{m}}$ as the halo annulus, and will indicate it with subscript A. The cross-power contribution of matter in these regions is then given by

$$P_{\mathrm{mA},i}(k) = \frac{f_{\mathrm{M},i,200\mathrm{m}} P_{\mathrm{mh},i,200\mathrm{m}}(k) - f_{\mathrm{M},i,500\mathrm{c}} P_{\mathrm{mh},i,500\mathrm{c}}(k)}{f_{\mathrm{M},i,200\mathrm{m}} - f_{\mathrm{M},i,500\mathrm{c}}}, \tag{10}$$

and the feedback-corrected annulus cross-contribution is then

$$P'_{\mathrm{mA},i}(k) = [f_{\mathrm{ret},i,200\mathrm{m}} f_{\mathrm{M},i,200\mathrm{m}} - f_{\mathrm{ret},i,500\mathrm{c}} f_{\mathrm{M},i,500\mathrm{c}}] P_{\mathrm{mA},i}(k). \tag{11}$$

When the annulus contribution can be calculated, we replace the regular $\Delta = 200\Omega_{\mathrm{m}}$ cross-power by $P'_{\mathrm{mh},i,200\mathrm{m}} = P'_{\mathrm{mh},i,500\mathrm{c}} + P'_{\mathrm{mA},i}$. As before, the fully corrected power contribution is then $P''_{\mathrm{mh},i,200\mathrm{m}} = q_{200\mathrm{m}} P'_{\mathrm{mh},i,200\mathrm{m}}$.

4.3 Model results

A proof of concept is presented in Fig. 9. On the left-hand side, we compare the true power suppression measured in B_AGN_W9 (red line) to the results of our model (orange, green, and blue-dashed lines). Our 'resummation' model takes as input halo baryon fractions measured from B_AGN_W9 for haloes $M_{500,\,\mathrm{crit}} > 10^{12}\,\mathrm{M}_{\odot}/h$ and combines these with quantities measured from DMO to predict the power suppression due to galaxy formation. Also shown is the result of applying the van Daalen et al. (2020) relation (cyan short dashed line), which uses only the baryon fraction measured for haloes around $M_{500,\,\mathrm{crit}} = 10^{14}\,\mathrm{M}_{\odot}/h$. While our model underpredicts the suppression on large scales when only $M_{500,\,\mathrm{crit}}$ haloes are used (orange), the agreement between the true suppression, and our model's prediction when using only $M_{200,\,\mathrm{mean}}$ haloes (green) is remarkable. When information from both overdensity regions is combined as described in subsection 4.2 (blue), the model reproduces the true suppression to < 1 per cent on all scales measured.

On the right-hand side of Fig. 9, we show the results of applying the same model to each of the cosmo-OWLS and BAHAMAS simulations explored in the previous sections, combining the $M_{500,\,\mathrm{crit}}$ and $M_{200,\,\mathrm{mean}}$ overdensity regions. We stress that for each simulation the exact same values for parameters a and b of equation (9) have been used; the only thing that changes from simulation to simulation are the baryon fractions measured in their haloes (and, when shifting between cosmo-OWLS and BAHAMAS, the DMO simulation used). The model typically reproduces the true power suppression to within 1 per cent accuracy all the way down to at least $k = 8\,h\,\mathrm{Mpc}^{-1}$, and almost always within 2 per cent. For the model with the strongest AGN feedback, B_AGNhigh_W9, the model slightly underpredicts the suppression on large scales, which again hints that haloes in this simulation may lose mass from regions larger than $r_{200,\mathrm{m}}$. However, even for this case the model is per cent level accurate. Following the procedure outlined in subsection 4.2, the model is easily extended to larger or smaller overdensity regions, such as $M_{2500,\,\mathrm{crit}}$, to cover an even larger range in k – as long as baryon fractions can be measured for these regions.

We note that the model is expected to perform slightly worse for cosmo-OWLS, since the DMO simulations of this suite model only a single fluid with a combined dark matter and baryon transfer function, whereas the baryonic simulations separate these into two fluids, and therefore also contain twice as many particles (see appendix B of van Daalen et al. 2020, for more information). Despite this, the model and simulations show remarkable agreement for this suite as well.

From the results presented in this work, it is clear why the van Daalen et al. (2020) relation (shown in cyan in the left-hand panel

[4] We note that $f_{\mathrm{ret},\,i,\,200\mathrm{m}}$ can be limited to a maximum value of 1 without changing the results presented here, but we find that $f_{\mathrm{ret},\,i,\,500\mathrm{c}}$ reaches values a few per cent higher than this for high-mass haloes.

Downloaded from https://academic.oup.com/mnras/article/528/3/4623/7590824 by Jacob Heeren user on 07 February 2025

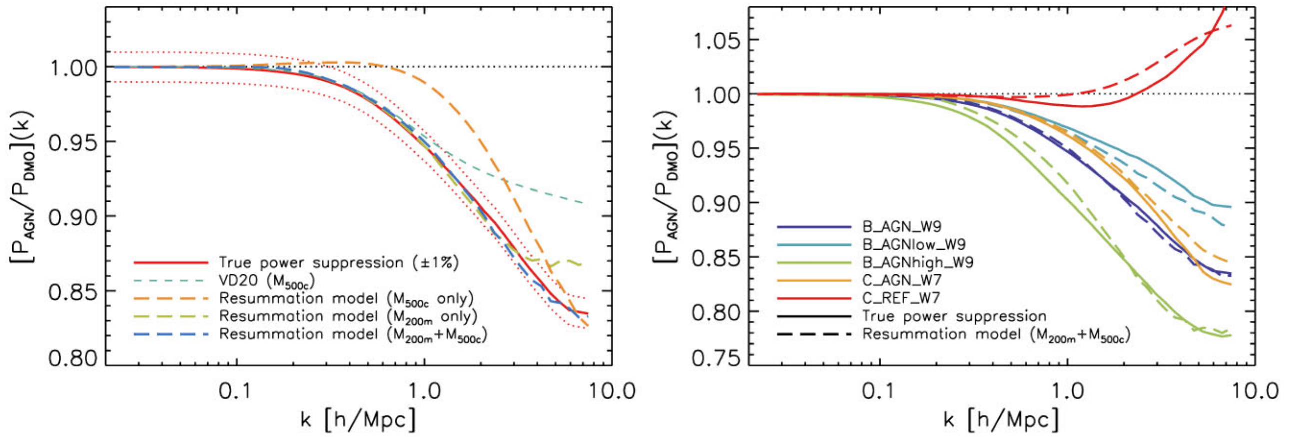

Figure 9. Left: The true power suppression of B_AGN_W9 (red) compared to what our 'resummation' model predicts. Combining information from both $r_{200,\mathrm{m}}$ and $r_{500,\mathrm{c}}$ gives the best results, although baryon fractions inside $r_{200,\mathrm{m}}$ alone are enough to reproduce the true suppression down to $k \approx 3\,h\,\mathrm{Mpc}^{-1}$ already. Also shown is the simple relation from van Daalen et al. (2020) (dashed cyan), which was fit to simulations up to $k = 1\,h\,\mathrm{Mpc}^{-1}$ and using only the baryon fraction at a single halo mass. Note that we set the suppression to unity for $k < 0.07\,h\,\mathrm{Mpc}^{-1}$ and smooth the result to counter sampling noise. Right: The same model applied to all simulations explored here. The 'resummation' model reproduces the true suppression to well within $1-2$ per cent on virtually all scales $k \leq 8\,h\,\mathrm{Mpc}^{-1}$, given baryon fractions as a function of halo mass, using only a single set of two fixed parameter values (see equation (9)).

of Fig. 9) was able to accurately fit the power suppression down to $k \approx 1\,h\,\mathrm{Mpc}^{-1}$ using the baryon fraction of $M_{500,\,\mathrm{crit}} \sim 10^{14}\,\mathrm{M}_{\odot}/h$ haloes: (a) the baryon fraction is strongly correlated with the retained mass fraction of haloes; (b) objects around this mass-scale dominate the power contributions on large scales; and (c) the effects of feedback in these haloes are generally highly correlated with those in adjacent mass scales. At the same time, this also makes it clear what the limitations of only using a single-baryon fraction are: the relation has to implicitly model the link between $10^{14}\,\mathrm{M}_{\odot}/h$ and other mass scales, capture its scaling with k, and be limited to scales roughly comparable to the size of the halo and above. The former two limitations also made the model less universally applicable, as the power suppression in simulations in which the relation between feedback effects on different mass scales deviated strongly from that of other models were more poorly reproduced (e.g. the original Illustris simulation, see Vogelsberger et al. 2014; van Daalen et al. 2020). In contrast, while the 'resummation' model presented here needs additional observationally determined baryon fractions as well as quantities measured from DMO simulations as input, it extends to higher k without losing accuracy, could straightforwardly be easily extended to higher redshifts, and has a far less empirical basis.

We have employed several implicit assumptions here, such as that feedback does not significantly change the halo positions or radii. The first is justified (see e.g. van Daalen et al. 2014) while the second is not (see e.g. Velliscig et al. 2014b), although it is unclear what the impact of this would be, if any. We also have assumed that the linear halo bias is preserved as haloes lose mass. We have checked this assumption by comparing the bias of matched haloes in our simulations, and found that the relative change in bias is typically $\lesssim 1$ per cent – but future iterations of this model could still take bias changes into account to further improve the performance. Another possible improvement is to reduce the scatter in the $f_{\mathrm{ret}} - f_{\mathrm{b}}$ relation by taking into account a possible halo mass dependence through the mass-dependent concentration of the haloes. As Elbers et al. (in preparation) will show, taking into account the baryon fraction and concentration simultaneously allows one to predict the power suppression more accurately. Still, from the results presented in Fig. 9, it would appear that our model is already able to yield highly accurate predictions despite these shortcomings.

5 SUMMARY AND DISCUSSION

In Section 3, we presented our findings concerning the contribution of haloes with a range of masses to the full power spectrum and the varying effects of baryons on the power in these haloes, when compared to a DMO simulation, as a function of scale using simulations from the cosmo-OWLS and BAHAMAS simulation projects. The contributions of various haloes to the full power spectrum and the baryon/DMO simulation power ratios of these haloes were considered for a matched (and an unmatched) set of haloes, their boundary defined by either their $r_{200,\mathrm{m}}$ or $r_{500,\mathrm{c}}$ spherical overdensity radius. These were compared to the results for the halo power within a constant SO radius between simulations. Lastly, the influences of variations in AGN feedback temperature on the contributions to the full power spectrum and the baryon/DMO simulation power ratios were also investigated for a matched set of haloes.

Our main findings are as follows:

(i) Haloes of around $M_{500,\,\mathrm{crit}} \sim 10^{14}\,\mathrm{M}_{\odot}/h$ provide the dominant contribution to the power spectrum up to $k \sim$ a few. Higher mass haloes provide a lesser but still very significant contribution on large scales ($k \sim 0.1\,h\,\mathrm{Mpc}^{-1}$), as their rarity becomes more important than their high masses and bias, while lower-mass haloes are less biased on large scales but provide a contribution comparable to $\sim 10^{14}\,\mathrm{M}_{\odot}/h$ haloes on smaller scales. This is in line with the findings of van Daalen & Schaye (2015). This also means that the effects of galaxy formation on these haloes are a strong indicator for how galaxy formation affects matter clustering as a whole, as found by van Daalen et al. (2020).

(ii) By matching haloes between baryonic and DMO simulations, we find that galaxy formation including AGN feedback lowers the masses within $r_{200,\mathrm{m}}$ of haloes down to at least $M_{500,\,\mathrm{crit}} \approx 10^{11.75}\,\mathrm{M}_{\odot}/h$, and therefore also their contributions to the power spectrum. On intra-halo scales, the removal of mass from clustered regions by AGN feedback ensures that the contribution of $r_{200,\mathrm{m}}$ overdensity regions to the power spectrum is smaller than that for a DMO universe up to at least $k = 10\,h\,\mathrm{Mpc}^{-1}$. Including galaxy formation but not AGN feedback also lowers all contributions, but by less than with AGN feedback, and only up to $k \sim$ a few, depending on halo mass.

Downloaded from https://academic.oup.com/mnras/article/528/3/4623/7590824 by Jacob Heeren user on 07 February 2025

(iii) The halo autopower for simulations with AGN shows a dip relative to DMO on scales $k \approx 10\,h\,\mathrm{Mpc}^{-1}$ for massive haloes ($M_{500,\,\mathrm{crit}} \gtrsim 10^{12.75}\,\mathrm{M}_{\odot}/h$), corresponding to scales internal to the haloes where mass was removed. For lower-mass haloes, this dip is not present, indicating that these haloes do not host (effective) AGN themselves but were affected by them indirectly. This could be due to nearby AGN heating and driving out the gas from these less massive haloes, or by them affecting the mass-accretion history of these haloes.

(iv) Even though the autopower contribution to the power spectrum from the same haloes goes down when AGN feedback is included, the peak fractional contribution of haloes $\gtrsim 10^{13.25}\,\mathrm{M}_{\odot}/h$ to the power spectrum is slightly higher than for DMO. This indicates that the contribution of cross-power between matter inside and outside $r_{200,\mathrm{m}}$ goes down on scales comparable to this radius.

(v) The choice of halo boundary ($r_{200,\mathrm{m}}$ or $r_{500,\mathrm{c}}$) affects the baryon/DMO power ratios for both massive and lower-mass haloes. Compared to DMO, baryonic haloes with masses $\leq 10^{12.75}\,\mathrm{M}_{\odot}/h$ lose a smaller fraction of their mass in their $r_{500,\mathrm{c}}$ regions than in their $r_{200,\mathrm{m}}$ regions, and the same goes for the most massive haloes ($M_{500,\,\mathrm{crit}} > 10^{14.25}\,\mathrm{M}_{\odot}/h$). However, haloes with masses $10^{12.75} \leq M_{500,\,\mathrm{crit}} \leq 10^{14.25}\,\mathrm{M}_{\odot}/h$, in which AGN are most effective, lose more mass from within $r_{500,\mathrm{c}}$ than within $r_{200,\mathrm{m}}$.

(vi) By fixing the $r_{500,\mathrm{c}}$ radius to the DMO value, we find that the autopower of haloes with $10^{12.25} \lesssim M_{500,\,\mathrm{crit}} \lesssim 10^{13.75}\,\mathrm{M}_{\odot}/h$ is increased compared to that within their own $r_{500,\mathrm{c}}$. The inverse is true for much more or much less massive haloes. This suggests that intermediate-mass haloes are dominated by mass ejection inside $\sim r_{500,\mathrm{c}}$, while more massive or lower-mass haloes are dominated by contraction.

(vii) The strength of AGN feedback primarily affects the normalization of the halo autopower contribution as a function of mass, on all scales probed here ($k < 10\,h\,\mathrm{Mpc}^{-1}$). Only for the most massive haloes, $M_{500,\,\mathrm{crit}} \gtrsim 10^{14}\,\mathrm{M}_{\odot}/h$, does the contribution significantly change shape for $k \gtrsim$ a few, as the AGN feedback affects the halo profiles on these scales.

Furthermore, in Section 4 we presented a novel model that utilizes the cross-power of halo matter inside spherical overdensity regions with all matter in combination with retained mass fractions to predict the suppression of the total power spectrum due to galaxy formation. We found that with a simple, fixed relation between observed halo baryon fractions and retained mass fractions our model can reproduce the power suppression of various simulations to ~ 1 per cent up to at least $k = 8\,h\,\mathrm{Mpc}^{-1}$. The best results were obtained if both $r_{200,\mathrm{m}}$ and $r_{500,\mathrm{c}}$ baryon fractions were available.

Compared to other models for the power suppression, such as halo-model-based approaches (e.g. Mead et al. 2015; Debackere et al. 2020; Mead et al. 2021), baryonification (e.g. Schneider & Teyssier 2015; Schneider et al. 2020; Aricò et al. 2021), and models built on fitting the power suppression of hydrodynamical simulations as a function of halo baryon fractions directly (e.g. van Daalen et al. 2020; Delgado et al. 2023; Salcido et al. 2023), our 'resummation' model (Section 4) has several advantages and disadvantages.

The model presented in this work is built on the link between the observed halo baryon fractions and the retained halo mass, rather than the overall suppression of power, and we find strong indications that this link may not (or only weakly) depend on the strength of feedback, allowing measurements of baryon fractions on different scales to set the power suppression in a model-independent way. There are currently also only two parameters present in our approach, both of which are fixed, and no halo profiles need to be modelled to get accurate predictions up to at least $k = 8\,h\,\mathrm{Mpc}^{-1}$, which means that cosmological parameters derived from weak lensing observations may have lower uncertainties than in most other approaches, as there are fewer parameters to marginalize over.

The main disadvantage is that our model is built on quantities derived from dark matter simulations, which require significant computational resources – although many of these already exist in the literature for the purposes of weak lensing analysis. However, similar to, for example baryonification, this shortcoming may be overcome in the future by training a model to produce the halo mass fractions and halo-matter cross-spectra outcomes for such relatively predictable simulations as a function of cosmology, or by using halo-model predictions. Exploring the dependence of our approach on cosmology, if any, may also lead to a significant reduction of resources, as fewer DMO simulations will be needed if the scaling with cosmology is known. Another disadvantage is that the model requires baryon fractions measured out to $r_{200,\mathrm{m}}$, which are less readily available than those within $r_{500,\mathrm{c}}$. While it is possible to predict one from the other, such a mapping would be model dependent. However, the availability of S-Z measurements of $\bar{f}_{\mathrm{b},200\mathrm{m}}$ is growing, so this may not be an issue for long.

Future work will extend the model presented in Section 4, including to $z > 0$, and apply it to the Gpc-scale FLAMINGO suite of simulations, recently presented in Schaye et al. (2023). As these simulations contain larger volumes with resolutions similar to BAHAMAS, as well as additional physics variations, analysing these simulations should lead to a more detailed modelling of the relation between the halo baryon and retained fractions, improving the accuracy of the model. Additionally, folding in other overdensity scales such as $r_{2500,\,\mathrm{crit}}$ or explicitly including galaxies through the measured stellar fractions of halo may allow us to extend the model to higher values of k.

ACKNOWLEDGEMENTS

We thank the authors of NBODYKIT, Nick Hand and Yu Feng, for making their code publicly available. MvD gratefully acknowledges support from the Netherlands Research Council NWO (VENI grant no. 639.041.748).

6 DATA AVAILABILITY

The data underlying this article will be shared on reasonable request to the corresponding author.

REFERENCES

Abbott T. M. C. et al., 2022, Phys. Rev. D, 105, 023520
Abdalla E. et al., 2022, Journal of High Energy Astrophysics, 34, 49
Ade P. A. R. et al., 2014, A&A, 571, 16
Aricò G., Angulo R. E., Hernández-Monteagudo C., Contreras S., Zennaro M., 2021, MNRAS, 503, 3596
Bond J., Cole S., Efstathiou G., Kaiser N., 1991, ApJ, 379, L440
Chisari N. E. et al., 2018, MNRAS, 480, 3962
Chisari N. E. et al., 2019, The Open Journal of Astrophysics, 2, 4
Colombi S., Jaffe A., Novikov D., Pichon C., 2009, MNRAS, 393, 511
Cooray A., Sheth R., 2002, Physics reports, 372, 1
Debackere S. N., Schaye J., Hoekstra H., 2020, MNRAS, 492, 2285
Delgado A. M. et al., 2023, MNRAS, 526, 5306
Duffy A. R., Schaye J., Kay S. T., Dalla Vecchia C., 2008, MNRASL, 390, L64
Duffy A. R., Schaye J., Kay S. T., Vecchia C. D., Battye R. A., Booth C., 2010, MNRAS, 405, 2161

Downloaded from https://academic.oup.com/mnras/article/528/3/4623/7590824 by Jacob Heeren user on 07 February 2025

Eisenstein D. J., Hu W., 1999, ApJ, 511, L5
Hand N., Feng Y., Beutler F., Li Y., Modi C., Seljak U., Slepian Z., 2018, AJ, 156, 160
Hearin A. P., Zentner A. R., Ma Z., 2012, JCAP, 2012, 034
Hellwing W. A., Schaller M., Frenk C. S., Theuns T., Schaye J., Bower R. G., Crain R. A., 2016, MNRASL, 461, L11
Heymans C. et al., 2021, A&A, 646, 140
Hinshaw G. et al., 2013, ApJS, 208, 19
Huterer D., Takada M., 2005, Astropart. Phys., 23, 369
Komatsu E. et al., 2011, ApJS, 192, 18
Laureijs R., 2009, preprint (arXiv:0912.0914)
Le Brun A. M., McCarthy I. G., Schaye J., Ponman T. J., 2014, MNRAS, 441, 1270
Lewis A., Challinor A., Lasenby A., 2000, ApJ, 538, L473
McCarthy I. G. et al., 2010, MNRAS, 406, 822
McCarthy I. G., Schaye J., Bower R. G., Ponman T. J., Booth C. M., Vecchia C. D., Springel V., 2011, MNRAS, 412, 1965
McCarthy I. G., Le Brun A., Schaye J., Holder G., 2014, MNRAS, 440, 3645
McCarthy I. G., Schaye J., Bird S., Le Brun A. M. C., 2017, MNRAS, 465, 2936
Mead A. J., Peacock J. A., Heymans C., Joudaki S., Heavens A. F., 2015, MNRAS, 454, 1958
Mead A. J., Brieden S., Tröster T., Heymans C., 2021, MNRAS, 502, 1401
Mummery B. O., McCarthy I. G., Bird S., Schaye J., 2017, MNRAS, 471, 227
Oppenheimer B. D., Babul A., Bah Y., Butsky I. S., McCarthy I. G., 2021, Universe, 7, 209
Pandey S. et al., 2023, MNRAS, 525, 1779
Peacock J., Smith R., 2000, MNRAS, 318, 1144
Planck Collaboration et al., 2016, A&A, 594, 13
Press W. H., Schechter P., 1974, ApJ, 187, L425
Salcido J., McCarthy I. G., Kwan J., Upadhye A., Font A. S., 2023, MNRAS, 523, 2247
Schaye J. et al., 2010, MNRAS, 402, 1536
Schaye J. et al., 2023, MNRAS, 526, 4978
Schneider A., Teyssier R., 2015, JCAP, 2015, 049
Schneider A., Teyssier R., Stadel J., Chisari N. E., Le Brun A. M. C., Amara A., Refregier A., 2019, JCAP, 2019, 020
Schneider A., Stoira N., Refregier A., Weiss A. J., Knabenhans M., Stadel J., Teyssier R., 2020, JCAP, 2020, 019
Seljak U., 2000, MNRAS, 318, 203
Semboloni E., Hoekstra H., Schaye J., 2013, MNRAS, 434, 148
Springel V., 2005, MNRAS, 364, 1105
Tinker J., Kravtsov A. V., Klypin A., Abazajian K., Warren M., Yepes G., Gottlöber S., Holz D. E., 2008, ApJ, 688, L709
van Daalen M. P., Schaye J., 2015, MNRAS, 452, 2247
van Daalen M. P., Schaye J., Booth C. M., Dalla Vecchia C., 2011, MNRAS, 415, 3649
van Daalen M. P., Schaye J., McCarthy I. G., Booth C. M., Dalla Vecchia C., 2014, MNRAS, 440, 2997
van Daalen M. P., McCarthy I. G., Schaye J., 2020, MNRAS, 491, 2424
Velliscig M., van Daalen M. P., Schaye J., McCarthy I. G., Cacciato M., Le Brun A. M., Vecchia C. D., 2014a, MNRAS, 442, 2641
Velliscig M., van Daalen M. P., Schaye J., McCarthy I. G., Cacciato M., Le Brun A. M. C., Dalla Vecchia C., 2014b, MNRAS, 442, 2641
Vogelsberger M. et al., 2014, MNRAS, 444, 1518
Vogelsberger M., Marinacci F., Torrey P., Puchwein E., 2020, Nature Rev. Phys., 2, 42
Wiersma R. P. C., Schaye J., Smith B. D., 2009, MNRAS, 393, 99

APPENDIX A: BOX-SIZE EFFECTS

When working with simulation data, there are numerical effects on the data that have no physical cause. One source of numerical effects is the limited size of the cosmological volume that is simulated. Apart from the limitation in scales that can be investigated, smaller boxes host fewer haloes disproportionally fewer rare systems, giving larger uncertainties in statistics.

Fig. A1 shows the contribution of haloes to the full power spectrum and the ratio of AGN/DMO power for a range of halo masses (the same range as used in the rest of the paper), for cosmo-OWLS simulations with volumes of $(400\,h^{-1}\mathrm{Mpc})^3$ (continuous lines), $(200\,h^{-1}\mathrm{Mpc})^3$ (dashed lines) and $(100\,h^{-1}\mathrm{Mpc})^3$ (dot-dashed lines). The resolution has been kept constant between the simulations. The haloes have been matched between the DMO and AGN simulations for each box size. The masses are based on the DMO simulation.

The top-left panel of the figure shows that for most mass bins, the different volumes broadly agree with one another on the contribution of different haloes above a certain mass to the full power spectra. The minor differences can be attributed to cosmic variance as they show no clear trend with increasing box size. The clear exception is the contribution of the most massive haloes ($M_{500,\,\mathrm{crit}} \geq 10^{14.75}\,\mathrm{M}_{\odot}/h$) to the full power spectrum in the L100 simulation (red dot-dashed line). This is because these haloes are so rare that they have difficulty forming in the L100 simulation and are therefore underrepresented. The fact that the L200 and L400 simulations converge on the vertical scale shows that these boxes are large enough to give a representational sample.

The bottom-left panel shows convergence for the lower masses ($M_{500,\,\mathrm{crit}} \lesssim 10^{13.75}\,\mathrm{M}_{\odot}/h$) between box sizes. The two highest mass bins show large discrepancies. Compensating for the lower contribution to the total of the most massive haloes ($M_{500,\,\mathrm{crit}} = 10^{14.5\pm0.25}\,\mathrm{M}_{\odot}/h$), the second most massive haloes ($M_{500,\,\mathrm{crit}} = 10^{14\pm0.25}\,\mathrm{M}_{\odot}/h$) have a higher contribution to the full power spectrum in the L100 simulation than in L200 or L400. While the L200 and L400 simulations agree on the contribution of $10^{14\pm0.25}\,\mathrm{M}_{\odot}/h$ haloes to the full power spectrum, the contribution of $10^{14.5\pm0.25}\,\mathrm{M}_{\odot}/h$ haloes to the total is higher in L200 than in L400. As they both agree on the contribution of haloes with $M_{500,\,\mathrm{crit}} \geq 10^{14.25}\,\mathrm{M}_{\odot}/h$ (top-left panel), it seems a few of the haloes with $M_{500,\,\mathrm{crit}} \geq 10^{14.75}\,\mathrm{M}_{\odot}/h$ in the L400 simulation are not fully formed in the L200 simulation, and added to the $10^{14.5\pm0.25}\,\mathrm{M}_{\odot}/h$ mass bin instead, increasing its contribution to the full power spectrum.

The right side of Fig. A1 shows the AGN/DMO power ratios for each halo mass bin for each volume. The top-right panel shows broad agreement when taking haloes with masses $\gtrsim 10^{13.5}\,\mathrm{M}_{\odot}/h$ into account. As seen in the left-hand panels however, AGN/DMO ratios of the most massive haloes do not agree across the various box sizes. For haloes with masses $\geq 10^{13.75}\,\mathrm{M}_{\odot}/h$ (orange), the depth of the characteristic dip varies with box size and smaller boxes place the minimum at lower k. Since there is no convergence in the scale at which the minimum of the dip is, larger boxes could still place it at larger k than the L400 simulation. For haloes with masses $\geq 10^{14.25}\,\mathrm{M}_{\odot}/h$ (red), the same can be said about the dip, where the AGN/DMO ratio for the L100 simulation deviates most, due to the under-representation. Comparing the L200 and L400 AGN/DMO ratios for this mass bin also shows a significant difference at $k \sim 2-3\,h\,\mathrm{Mpc}^{-1}$, where the small peak in the AGN/DMO ratio is higher (by ≈0.02).

The bottom-right panel shows a large discrepancy for the lowest two-halo mass bins ($M_{500,\,\mathrm{crit}} = 10^{11.5\pm0.25}\,\mathrm{M}_{\odot}/h$, pink and $M_{500,\,\mathrm{crit}} = 10^{12\pm0.25}\,\mathrm{M}_{\odot}/h$, purple) between the L200 simulation and the other two box sizes for $k \lesssim 8\,h\,\mathrm{Mpc}^{-1}$. There seems to be much less mass-loss due to AGN feedback in these haloes in the L200 simulation. Note that these haloes border on the resolution limits. Apart from the most massive haloes, previously discussed, the AGN/DMO ratios for the other halo masses agree quite well.

Downloaded from https://academic.oup.com/mnras/article/528/3/4623/7590824 by Jacob Heeren user on 07 February 2025

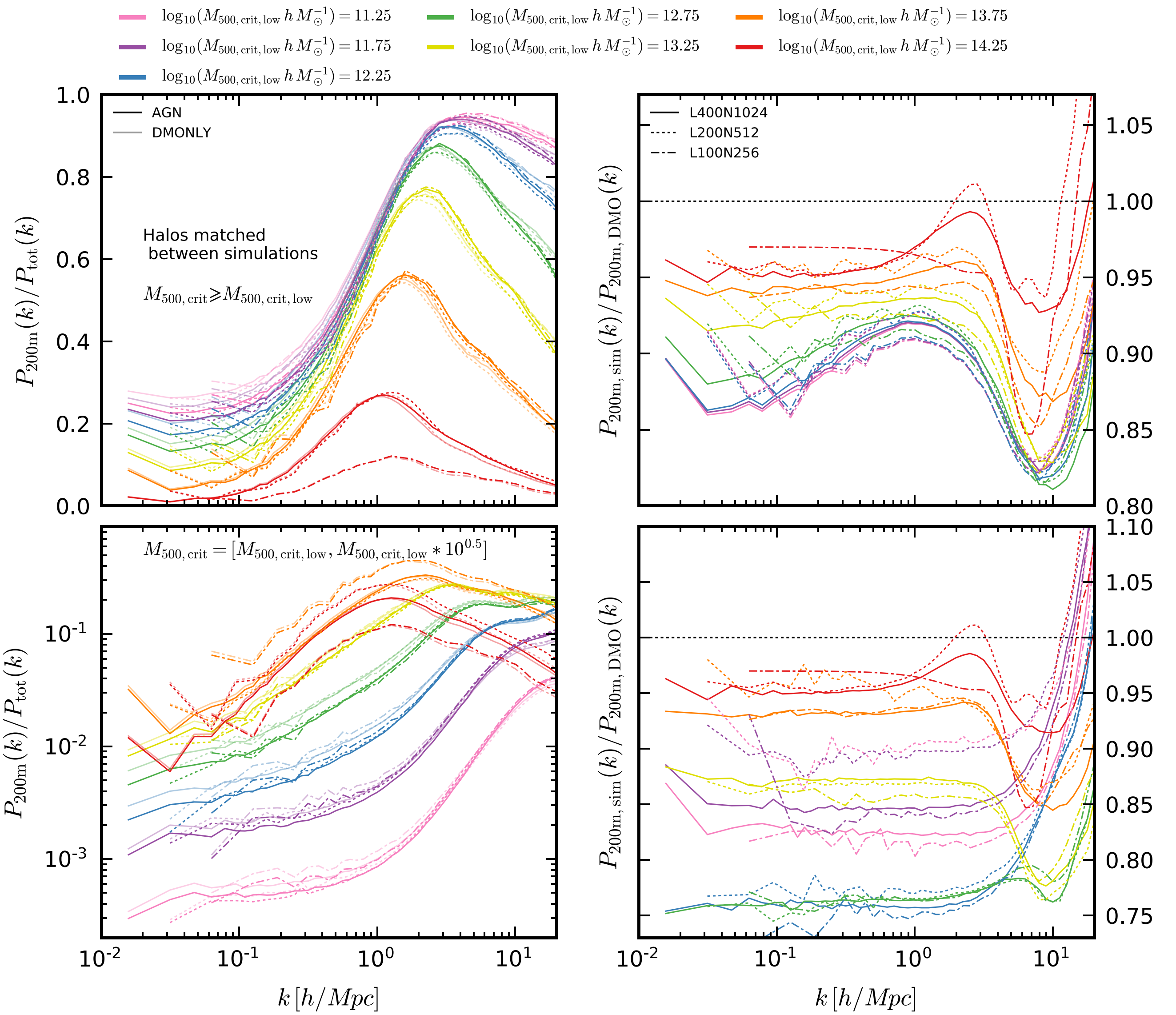

Figure A1. Similar to Fig. 4, except that not only the L400N1024 (continuous), but also the L200N512 (dashed), and the L100N256 (dot-dashed) cosmo-OWLS simulations are shown. The resolution of all simulations is kept fixed as the box size is varied. The largest deviations between the different box sizes are in the most massive haloes, due to cosmic variance being large for these in smaller volumes.

As the deviations for the most massive haloes are likely due to the rarity of these haloes, we conclude that a $(400\,h^{-1}\,\mathrm{Mpc})^3$ is a minimum requirement for this study.

APPENDIX B: COSMOLOGY

Recall from Section 1, that the cosmological model parameters influence the power in numerous ways, as they effect halo collapse, formation and evolution, the amount of matter available and the initial power spectrum, resulting, for example, in a different halo mass distribution. To learn how this translates through into the power spectrum and which haloes are most influenced by these changes is crucial, considering the upcoming weak lensing surveys that allow for precision cosmology (see Section 1).

Fig. B1 shows that both the contribution of haloes, defined by particles within $r_{200,\mathrm{m}}$, to the full power spectrum and the ratio between AGN and DMO for haloes in the usual range of masses are dependent on cosmology, at $z = 0$. For both the WMAP9 (continuous) and the *Planck* (dashed) simulations the haloes have been matched between AGN and DMO. Furthermore, the two DMO simulations (B_DMO_W9 and B_DMO_PL) are also matched, to ensure that every line in Fig. B1 of a certain colour (mass bin) is based on the same haloes and can thus be compared. The halo masses as shown in the legend (the same range as in earlier figures) are based on B_DMO_W9.

On large scales, the top-left panel shows that the fraction of mass in the massive haloes is similar between the cosmologies. As more lower-mass haloes are added, the the fraction of mass in haloes in the DMO simulation (transparent) rises above that in the AGN simulations (solid), as in earlier figures, but the two cosmologies broadly agree. The *Planck* cosmology produces slightly more massive haloes for both B_AGN_PL and B_DMO_PL, due to a higher Ω_m and a lower h, but the top panel in Fig. B1 shows that the fraction of the total mass in these haloes is also

Downloaded from https://academic.oup.com/mnras/article/528/3/4623/7590824 by Jacob Heeren user on 07 February 2025

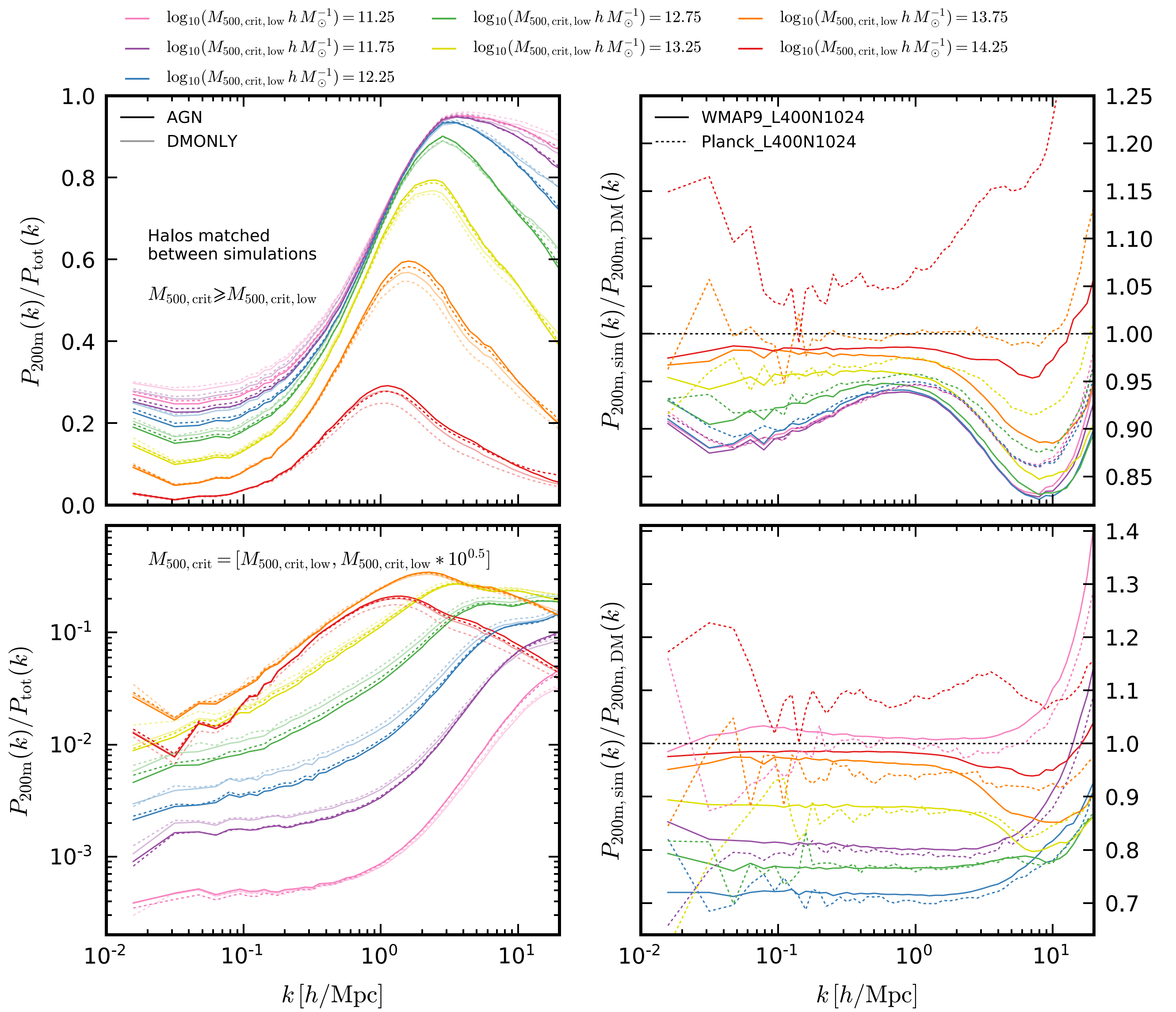

Figure B1. Similar to Fig. 7, except that the B_AGN_PL and B_DMO_PL (dashed) have been added to the B_AGN_W9 and B_DMO_W9 (continuous) power spectra to allow for a comparison between cosmologies. Both AGN-DMO simulation pairs have been matched and the two DMO simulations have also been matched. The halo mass bins are based on B_DMO_W9. The influence of cosmology on the contributions of halo power to the full power spectrum and the AGN/DMO ratios of halo power is largest for massive haloes ($M_{500,\rm crit} \gtrsim 10^{13.25}\,\rm M_\odot/h$). Furthermore, the *Planck* cosmology moves power from massive to lower-mass haloes, when compared to the WMAP9 cosmology.

a slightly larger. This is verified by the bottom-left panel, where the contribution of power in the haloes in the *Planck* simulation to the full power spectrum is higher for all mass bins in both B_AGN_PL and B_DMO_PL, with the exception of the most massive haloes ($M_{500,\rm crit} = 10^{14.5\pm0.25}\,\rm M_\odot/h$, red lines) in B_DMO_PL and the lowest mass haloes ($M_{500,\rm crit} = 10^{11.5\pm0.25}\,\rm M_\odot/h$, pink lines) in both B_AGN_PL and B_DMO_PL, the latter having a low matching fraction (see Fig. 1), thus calling for caution when interpreting.

Moving to the scales where the 1-halo term takes over ($k \gtrsim k_{\rm peak}$), the top-left panel of Fig. B1 shows a variation with minimal halo mass in the discrepancies between the two cosmologies in the contribution of halo power to the full power spectrum. When considering only massive haloes ($M_{500,\rm crit} \gtrsim 10^{13.5}\,\rm M_\odot/h$), the discrepancies between the WMAP9 (continuous) and *Planck* (dashed) contributions to the full spectrum are quite substantial, where the contributions of the haloes to the full spectrum in the *Planck* simulations are lower than in the WMAP9 simulations for both DMO and AGN. Adding lower-mass haloes diminishes these discrepancies, until the roles of the halo power contributions to the total of both cosmologies are reversed and the halo power contributions to the *Planck* simulations rise above those to the WMAP9 simulations. This relative position shift of the two cosmologies happens when haloes with masses $\lesssim 10^{12.75}\,\rm M_\odot/h$ are added. This indicates that there is more power in haloes in the *Planck* simulations and that power that is in massive haloes in the WMAP9 simulation, has been moved to the lower-mass haloes in the *Planck* simulation. This is likely due to shifts in the halo mass function between these cosmologies.

For the highest mass haloes ($M_{500,\rm crit} \geq 10^{13.25}\,\rm M_\odot/h$, yellow, orange and red), for $k \gtrsim 1\,h\,\rm Mpc^{-1}$, the differences between the two cosmologies are most striking, as can be seen in the top-left and top-

Downloaded from https://academic.oup.com/mnras/article/528/3/4623/7590824 by Jacob Heeren user on 07 February 2025

right panels of Fig. B1. Next to the previously discussed vertical displacement between the two cosmologies in the top-left panel there is also a vertical displacement in the AGN/DMO power ratios. Moreover, the $10^{14\pm0.25}\,\mathrm{M}_\odot/h$ haloes (orange lines) show the characteristic dip in the AGN/DMO ratio in the WMAP9 simulation around $k \sim 8\,h\,\mathrm{Mpc}^{-1}$ but remain nearly constant for the *Planck* simulation (bottom-right panel). Comparing the $M_{500,\,\mathrm{crit}} \geq 10^{13.75}\,\mathrm{M}_\odot/h$ *Planck* (orange-dashed line) and the $M_{500,\,\mathrm{crit}} \geq 10^{14.25}\,\mathrm{M}_\odot/h$ WMAP9 (red continuous line) AGN/DMO power ratios in the top-right panel of Fig. B1, reveals these haloes to both omit the characteristic dip around $k \sim 8\,h\,\mathrm{Mpc}^{-1}$, which shows the reaction of the haloes to the AGN feedback. The AGN/DMO ratios of these two mass bins are very similar to one another. This suggests that the potential wells of these haloes in the *Planck* simulation are so deep, that they resemble the $10^{14.5\pm0.25}\,\mathrm{M}_\odot/h$ haloes in the WMAP9 simulation. In the *Planck* simulation the $10^{14\pm0.25}\,\mathrm{M}_\odot/h$ haloes have grown more massive than in the WMAP9 simulation (due to the higher Ω_m and lower h), ending up to be around the size of the $10^{14.5\pm0.25}\,\mathrm{M}_\odot/h$ haloes in WMAP9. For these group-sized haloes ($10^{14\pm0.25}\,\mathrm{M}_\odot/h$), cosmology is a very important factor in their formation, growth and structure. This is also visible, albeit to a lesser degree, in the bottom-right panel of Fig. B1.

The most massive haloes have an AGN/DMO power ratio >1 in the *Planck* simulation, which is unlikely to be a consequence of bad matching alone, as the matched fraction for these haloes is >0.95. This ratio therefore seems to suggest that these haloes have grown so massive that baryonic feedback does not suppress the power at all. However, even this small deviation from unity in the matched fraction means that there may be a misrepresentation of haloes, which can for example be due to mergers of very massive haloes where the matching has chosen only one of the two haloes, and omitted the other from the set. As very massive ($M_{500,\,\mathrm{crit}} \geq 10^{14.25}\,\mathrm{M}_\odot/h$) haloes are not abundant ($\sim 10^2$), this can impact the results substantially.

The bottom-right panel indicates that the DMO/AGN ratios of haloes with masses $\lesssim 10^{13.25}\,\mathrm{M}_\odot/h$ are only slightly influenced by cosmology, whereas the massive haloes have a much stronger dependence.

In conclusion, cosmology clearly impacts the power contribution of haloes and their AGN/DMO power ratios. The influence of cosmology is much more substantial for the most massive haloes, in their formation and evolution as well as in the influence of AGN feedback on their power suppression in the AGN simulations, when compared to the DMO simulations. As there are many factors that are influenced by cosmology that determine the power in different mass haloes, more extensive research is required to disentangle the effects of the various cosmological parameters and find the one(s) dominating the changes in power.

This paper has been typeset from a TEX/LATEX file prepared by the author.

Downloaded from https://academic.oup.com/mnras/article/528/3/4623/7590824 by Jacob Heeren user on 07 February 2025

© 2024 The Author(s)
.Published by Oxford University Press on behalf of Royal Astronomical Society. This is an Open Access article distributed under the terms of the Creative Commons Attribution License (https://creativecommons.org/licenses/by/4.0/), which permits unrestricted reuse, distribution, and reproduction in any medium, provided the original work is properly cited